HHS Public Access

Author manuscript

Cancer Immunol Res. Author manuscript; available in PMC 2020 June 01.

Published in final edited form as:

Cancer Immunol Res. 2019 December ; 7(12): 2036–2051. doi:10.1158/2326-6066.CIR-19-0152.

Trabectedin reveals a strategy of immunomodulation in chronic lymphocytic leukemia

Priyanka Banerjee[1,9], **Ronghua Zhang**[1], **Cristina Ivan**[1], **Giovanni Galletti**[1,10], **Karen Clise-Dwyer**[2], **Federica Barbaglio**[3], **Lydia Scarfò**[3,4], **Miguel Aracil**[5], **Christian Klein**[6], **William Wierda**[7], **William Plunkett**[1], **Federico Caligaris-Cappio**[8,11], **Varsha Gandhi**[1], **Michael J. Keating**[7], **Maria Teresa S. Bertilaccio**[1]

[1]Department of Experimental Therapeutics, The University of Texas MD Anderson Cancer Center, Houston, Texas, USA [2]Department of Stem Cell Transplantation & Cellular Therapy, The University of Texas MD Anderson Cancer Center, Houston, Texas, USA [3]B-cell Neoplasia Unit, Division of Experimental Oncology, IRCCS San Raffaele Scientific Institute, Milan, Italy [4]Università Vita-Salute San Raffaele, Milan, Italy [5]R&D, PharmaMar, Madrid, Spain [6]Roche Pharma Research and Early Development, Oncology Discovery, Roche Innovation Center Zurich, 8952 Zurich, Switzerland [7]Department of Leukemia, The University of Texas MD Anderson Cancer Center, Houston, Texas, USA [8]Division of Experimental Oncology, IRCCS San Raffaele Scientific Institute, Milan, Italy [9]P.B. is presently at Houston Methodist Research Institute, Houston, Texas, USA [10]G.G. is presently at Humanitas Clinical and Research Center, Rozzano, Milan, Italy [11]F.C.-C. is presently the scientific director of AIRC (Associazione Italiana per la Ricerca sul Cancro), 20123 Milan, Italy

Abstract

Chronic lymphocytic leukemia (CLL) is a B-cell neoplasia characterized by pro-tumor immune dysregulation involving non-malignant cells of the microenvironment, including T lymphocytes and tumor-associated myeloid cells. Although therapeutic agents have improved treatment options for CLL, many patients still fail to respond. Some patients also show immunosuppression. We have investigated trabectedin, a marine-derived compound with cytotoxic activity on macrophages in solid tumors. Here we demonstrate that trabectedin induces apoptosis of human primary

Corresponding author: Maria Teresa Sabrina Bertilaccio, ORCID 0000-0002-2304-4618, Department of Experimental Therapeutics, The University of Texas MD Anderson Cancer Center, Houston, Texas, USA, 1901 East Road, Houston, TX 77054, MSBertilaccio@mdanderson.org, Phone: +1-713-563-6128, Fax: +1 713-745-9231.

AUTHOR CONTRIBUTIONS

P.B. performed experiments, analyzed the data and reviewed the paper; R.Z. performed experiments and analyzed the data; C.I. performed the statistical analysis of the data and reviewed the paper; G.G. performed experiments and analyzed the data; K.C-K. assisted in flow cytometry and cell sorting study design, set up and analysis; F.B. performed in vitro studies; L.S. contributed patient samples with clinical/biological features and assisted in human studies; M.A.A. provided trabectedin and assisted in trabectedin studies; C.K. provided moAb and assisted in anti-CD20 studies; W.W. contributed patient samples with clinical/biological features and assisted in the discussion of the results; W.P. assisted in the discussion and interpretation of the results; F.C.-C. initially guided the research, assisted in the interpretation and discussion of the results and reviewed the paper; V.G. assisted in the interpretation and discussion of the results and reviewed the paper; M.J.K. contributed patient samples with clinical/biological features, provided patient-related input, assisted in the interpretation and discussion of the results; M.T.S.B. designed and supervised the project, performed experiments, analyzed the data and wrote the paper.

PB and RZ contributed equally to this work

Conflict of interest disclosure : M.A.A. is employee of PharmaMar, C.K. is employee of Roche. All the remaining authors declare no competing financial interests

leukemic cells and also selected myeloid and lymphoid immunosuppressive cells, mainly through the TRAIL/TNF pathway. Trabectedin modulates transcription and translation of IL-6, CCL2 and IFNα in myeloid cells and FOXP3 in regulatory T cells. Human memory $CD8^+$ T cells downregulate PD-1 and, along with monocytes, exert in vivo antitumor function. In xenograft and immunocompetent CLL mouse models, trabectedin has anti-leukemic effects and antitumor impact on the myeloid and lymphoid cells compartment. It depletes myeloid- derived suppressor cells and tumor-associated macrophages and increases memory T cells. Trabectedin also blocks PD-1/PD-L1 axis by targeting $PD\text{-}L1^+$ CLL cells, $PD\text{-}L1^+$ monocytes/macrophages, and $PD\text{-}1^+$ T cells. Thus trabectedin behaves as an immunomodulatory drug with potentially attractive therapeutic value in the subversion of the protumor microenvironment and in overcoming chemoimmune resistance.

Keywords

chronic lymphocytic leukemia; trabectedin; immunomodulation; B-cells; myeloid-cells

INTRODUCTION

Introduction of therapeutic agents including kinase and BCL-2 inhibitors has improved treatment options for patients with chronic lymphocytic leukemia (CLL), although some patients fail to respond, become resistant or relapse during treatment (1–3). Patients with lymphoid malignancies receiving Bruton's tyrosine kinase inhibitor, ibrutinib, are at risk of infection, including lethal invasive fungal infections (4), likely due to the inhibition of innate immune surveillance (5). Fludarabine-based chemo-immune therapy remains the frontline therapy for many patients, although the cytotoxic activity that fludarabine has against leukemic cells is accompanied by damage to normal immune cells, which leads to immune dysfunction and opportunistic infections (6–10). Alternative strategies are needed to bypass mechanisms that contribute to CLL cell resistance and immune dysfunction and to improve CLL patients' quality of life.

Leukemic cells depend on survival signals provided by microenvironment non-neoplastic cells (11). As in solid tumors, these signals enhance the frequency of immunosuppressive cells, including regulatory T cells (Treg)(12), tumor-associated macrophages (13) and myeloid derived suppressor cells (14).

In CLL, T lymphocytes exhibit exhaustion and functional defects (15) (e.g. impaired immunologic synapse formation and reduced cytotoxic capacity).

Clinical trials of CD19 chimeric antigen receptor (CAR) T cell therapy revealed resistance in CLL patients likely due to T-cell defects that are characteristic of CLL and worsen with disease progression (16).

The CLL microenvironment is characterized by an excess of $CD4^+CD25^+Foxp3^+$ Treg cells that are resistant to apoptosis likely due to high Bcl-2 expression (17). $CD4^+$ T cells seem to provide a niche that favors development and maintenance of the disease (18). Another component of the immune microenvironment is represented by nurse-like cells (NLCs) that

in vitro promote CLL cell survival mainly through SDF1 (19). NLCs resemble macrophages and have been identified as CLL-specific tumor-associated macrophages (TAMs) (20).

We demonstrated in CLL mouse models that TAMs support survival and proliferation of CLL and can be therapeutically targeted by CSF1R signaling blockade to restore leukemic cells' apoptosis sensitivity. Macrophage targeting via CSF1R inhibition reprograms the tumor microenvironment toward an antitumor phenotype by activating effector memory T cells and reducing immunosuppressive cells of the lymphoid and myeloid lineage such as Treg cells and monocytic-myeloid derived suppressor cells (M-MDSCs) (13). These findings indicate bidirectional crosstalk between CLL cells, MDSCs and Treg cells (14).

These observations led us to investigate ET-743/trabectedin, a DNA binding sea squirt-derived compound, known to target TAMs in solid tumors. Trabectedin is approved for treatment of soft-tissue sarcoma (21) and ovarian cancer (22). Unlike conventional chemotherapeutic agents (23), trabectedin binds the minor groove of DNA, blocks the cell cycle, affects gene transcription and DNA repair pathways (24, 25), and is a transcription-coupled nucleotide excision repair (TC-NER) agent. The targeting of TC-NER induces selective CLL cell death, regardless of genotype or preceding therapies (26). Trabectedin affects transcription regulation of cancer cells and some normal cells of the tumor microenvironment, which produce cytokines and factors promoting tumor growth (25). In solid tumors, trabectedin shows activity against tumor-associated myeloid cells (23, 27) and other immune cells (25, 28). In sarcoma, trabectedin targets cancer cells, shows selective TRAIL-mediated cytotoxicity against human monocytes, and inhibits the production of cytokines such as CCL2 and IL-6 (29). We therefore hypothesized that trabectedin synergistically targets both leukemic cells and non-malignant microenvironment cells. This study uncovered the immunomodulatory function of trabectedin in CLL. We showed that at very low doses this drug repairs the immune system and kill leukemic cells.

METHODS

Cells and reagents

For cell viability studies, human primary samples were obtained from CLL patients (RAI stage 0–2), who provided informed consent as approved by the Institutional Ethical Committee (protocol VIVI-CLL) of San Raffaele Scientific Institute (Milan, Italy) in accordance with the Declaration of Helsinki. For all the other studies with human blood samples, specimens were obtained from CLL patients (any RAI stages) referred to the Leukemia Department at M.D. Anderson Cancer Center with the approval of MD Anderson's Institutional Review Board (protocol 2014–0678), in accordance with the Declaration of Helsinki. Written informed consent was obtained from the donors. The clinical and biological features of CLL patients analyzed are described in Supplementary Tables S1 and S2.

MEC1 cells are a $CD5^{low/-}$ CLL cell line established from a CLL patient in prolymphocytoid transformation to B-PLL, obtained from Deutsche Sammlung von Mikroorganismen und Zellkulturen (DMSZ, Braunschweig, Germany) and cultured in RPMI 1640 medium (Invitrogen, Carlsbad, CA, USA) with 10% fetal bovine serum and gentamicin

(15 μg/mL; Sigma-Aldrich, St. Louis, MO, USA). MEC1 cells have been obtained in 2014 from DSMZ, they were cultured for 1–2 weeks and frozen at low passages (5–10). For in *in vitro* and *in vivo* experiments MEC1 cells were thawed, cultured for 1–2 weeks and used at 15–20 passages. MEC1 cell lines regularly tested negative for *Mycoplasma* contamination (PCR mycoplasma detection kit, Applied Biological materials Inc., Richmond, BC, Canada) and have not been reauthenticated in the past year. Trabectedin (Yondelis) was provided by Pharma Mar (Madrid, Spain), S.A., Sociedad Unipersonal. For in vitro studies trabectedin as pure powder was dissolved in DMSO to 1mM and kept at −20°C. For in vivo studies trabectedin was provided as sterile lyophilized powder (including sucrose, potassium dihydrogen phosphate, phosphoric acid and potassium hydroxide) and dissolved in physiologic solution, following the preparation guide for patient infusion of Yondelis. A monoclonal antibody (moAb) to human CD20 (GA101, ref, (30) was provided by Roche Innovation Center Zurich, Switzerland.

Cytotoxicity assay

Human primary $CD19^+$ cells and MEC1 cells were seeded in 96-well plates at a concentration of 3×10^6 cells/mL in 0.2 mL of RPMI. Vehicle (DMSO) as control and increasing concentrations of trabectedin (0.001 μM, 0.01 μM, 0.1 μM, 1 μM, 10 μM) were added, and cell viability was assessed at different 24h, 48h, and 72h) using CellTiter-Glo chemoluminescence assay (Promega, Madison, WI, USA).

In vitro cultures and quantitative flow cytometry-based cell-depletion assay from CLL patient samples

Depending on the experiments, fresh peripheral blood mononuclear cells (PBMCs) or $CD19^+$ cells from untreated CLL patients were seeded, in triplicate, at 3×10^6 cells/ml in culture medium and treated with trabectedin (0.01 μM) or DMSO vehicle for 24h, in the presence or absence of anti-TRAIL-R2 (human, 1μg/ml) moAb (HS201) from Adipogen AG (San Diego, CA, USA). The specific percentages of remaining cells in the treated samples were calculated as (the absolute number of cells in treated samples/the absolute number of cells in control samples) x 100. For each condition, the absolute number of remaining cells was calculated as the total number of viable cells (trypan blue exclusion determination) x the percentage of viable cells (flow cytometry analysis determination). Then, specific cell depletion was calculated as [100 - the specific percentage of remaining cells], as described (13). The flow cytometry analysis of human myeloid and lymphoid cell types is described below and in Supplementary Tables S3–S7. For transcriptional studies, fluorescence-activated cell sorting was performed after 15 h of trabectedin treatment (described below and in Supplementary Table S8).

Human cell purification, flow cytometry, and cell sorting

For cytotoxicity studies, leukemic cells were purified immediately after blood withdrawal, by negative depletion, using a B-lymphocyte enrichment kit (RosetteSep; STEMCELL Technologies, Vancouver, BC, Canada). The purity of all preparations was more than 99%, and the cells coexpressed CD19 and CD5 on their cell surfaces as assessed by flow cytometry; preparations were virtually devoid of natural killer cells, T lymphocytes, and monocytes. Phenotype analysis of human MEC1 leukemic cells in xeno-transplanted mice

was performed with PE-Cy7 Mouse Anti-Human CD19 (J3–119) purchased by Beckman Coulter (Brea, CA, USA). Surface expression was analyzed using Cytomics FC500 (Beckman Coulter).

For *in vitro* cell depletion assays, 8-color flow cytometry phenotype analysis of human live myeloid cells and 11-color flow cytometry phenotype analysis of human live lymphoid cells were performed using LSRFortessa X-20 (BD Biosciences, San Jose, CA, USA).

PBMCs were first incubated with LIVE/DEAD fixable Aqua dye (Thermo Fisher Scientific, Waltham, MA, USA); then, after the blocking of Fc receptors, the cells were stained with the surface antibodies described in Supplementary Table S3 and Supplementary Table S4. Finally, the cells were incubated with ammonium chloride solution (STEMCELL Technologies) to lyse red cells. For lymphoid cell Foxp3 detection, surface-stained cells were further fixed and permeabilized using a Treg detection Kit (Miltenyi Biotec, Bergisch Gladbach, Germany) and finally stained with an anti-Foxp3 antibody.

For transcriptional and patient-derived xenograft studies, live myeloid cells were isolated by 4-way fluorescence-activated cell sorting on a BD FACS Aria II (BD Biosciences), after surface staining with the following antibodies: Alexa Fluor 700 mouse anti-human CD66b (G10F5), APC mouse anti-human Lineage Cocktail (CD3/CD19/CD20/CD56) (UCHTI, HIB19, 2H7, 5.1H11), Brilliant Violet 786 mouse anti-human CD14 (MφP9) purchased by BD Biosciences, PE mouse anti-human CD16 (3G8) purchased by Biolegend (San Diego, CA, USA), APC-Cy7 mouse anti-human HLA DR (L243).

Live lymphoid cells were isolated by 4-way fluorescence-activated cell sorting on a BD FACS Aria II after surface staining with the following antibodies: eFluor 450 mouse anti-human CD8a (SK1) purchased by eBiosciences (Waltham, MA, USA), PerCP mouse anti-human CD45RO (UCHL1) purchased by Biolegend, PE-Cy7 mouse anti-human CD45RA (L48) purchased by BD Biosciences, Brilliant Violet 605 mouse anti-human CD62L (DREG-56), PE-Dazzle 594 mouse anti-human CD4 (SK3), PE mouse anti-human CD25 (4E3) purchased by Milteny Biotec, APC mouse anti-human CD19 (J3–119) purchased by Beckman Coulter, FITC mouse anti-human CD127 (HIL-7R-M21) purchased by BD Biosciences. Live/Dead Fixable Aqua (Thermo Fisher Scientific) staining was first performed to allow the discrimination of Live/Dead cells.

Samples were analyzed with FCS Express 6 Flow Cytometry Software (De Novo Software, Glendale, CA, USA). Monocyte subsets have been identified by a negative exclusion gating strategy (31, 32). We excluded $CD66b^+$ neutrophils, then, using a lineage (Lin) cocktail including moAbs to CD3, CD19, CD20 and CD56, we excluded T cells, B cells, and NK cells, respectively. CD14 and CD16 expression was then used to identify $CD14^+CD16^{++}$ non classical (NC), $CD14^{++}CD16^+$ intermediate (I) and $CD14^{++}CD16^-$ classical (C) monocytes. T cells have been identified as follows: naïve $hCD8^+$ $CD45RO^-CD45RA^+CD62L^+$ T cells, central memory $hCD8^+$ $CD45RA^-CD45RO^+CD62L^+$ T_{CM}, effector memory $hCD8^+$ $CD45RA^-CD45RO^+CD62L^-$ T_{EM}.

Intracellular cytokine detection on human myeloid cells

For the detection of IFNα, TNFα, IL-12, IL-6, and CCL2 on human myeloid cells, fresh PBMCs from CLL patients were seeded at 1×10^6 cells/ml in culture medium and treated with trabectedin (0.01 μM) or DMSO vehicle for 15h or 38h. Then, they were stimulated in vitro with ionomycin and Brefeldin A, and stained with the following surface antibodies: Alexa Fluor 700 mouse anti-human CD66b (G10F5), APC mouse anti-human Lineage Cocktail (CD3/CD19/CD20/CD56) (UCHTI, HIB19, 2H7, 5.1H11), Brilliant Violet 786 mouse anti-human CD14 (MφP9) purchased by BD Biosciences, BUV737 mouse anti-human CD16 (3G8) purchased by BD Biosciences, PE mouse anti-human TRAIL-R2 purchased by BioLegend. The IntraPrep Permeabilization Kit (Beckman Coulter) was used for the intracellular detection of the cytokines described in Supplementary Table S5. Live/Dead Fixable Aqua (Thermo Fisher Scientific) staining was first performed to allow the discrimination of Live/Dead cells. Samples were acquired using an LSRFortessa X-20 and analyzed with FCS Express 6 Flow Cytometry Software.

Violet proliferation dye (VPD)-based phagocytosis assay

MEC1 cells were labelled with Calcein-Violet-AM proliferation dye (VPD, BioLegend) and co-cultured with monocytes at effector target ratio 1:1 in the presence or absence of 0.01μM trabectedin for 16h. To distinguish between phagocytosed VPD-positive MEC1 cells and free MEC1 cells, samples were counterstained with the following surface antibodies: anti-human CD66b, anti-human Lineage Cocktail (CD3/CD19/CD20/CD56), anti-human CD14 and anti-human CD68 antibody. The IntraPrep Permeabilization Kit (Beckman Coulter) was used for the intracellular detection of the CD68 macrophage marker. After the exclusion of neutrophils (through CD66b molecule), and then the exclusion of NK/NKT cells, T cells, and B cells (through lineage cocktail including CD56, CD3, CD19, CD20 molecules), VPD^+ $CD14^-$ cells and VPD^+ $CD68^-$ cells were identified by flow cytometric analysis. The absolute number of surviving VPD^+ $CD68^-$ target cells and of VPD^+ $CD14^-$ target cells were calculated. The percentage of trabectedin-mediated phagocytosis by $CD68^+$ macrophages was calculated using the previously described (33) formula: % trabectedin-mediated phagocytosis = 100 – ((absolute number of surviving VPD^+ $CD68^-$ MEC1 cells in the presence of trabectedin/absolute number of surviving VPD^+ $CD68^-$ MEC1 cells in the absence of trabectedin)x100%). The percentage of trabectedin-mediated phagocytosis by $CD14^+$ monocytes was calculated using the formula: % trabectedin-mediated phagocytosis = 100 – ((absolute number of surviving VPD^+ $CD14^-$ MEC1 cells in the presence of trabectedin/absolute number of surviving VPD^+ $CD14^-$ MEC1 cells in the absence of trabectedin)x100%). The antibodies used in this assay are described in Supplementary Table S6.

Human T cell *in vitro* functional assay and cytokine detection

$CD8^+$ T lymphocytes (including $hCD8^+$ T_{EM} and $hCD8^+$ T_{CM}) were separated by fluorescence-activated cell-sorting, co-incubated in vitro at effector target ratio 2:1 with MEC1 cells heated at 47°C for 1h to induce tumor-antigen specific T cell response (Ag-experienced) (34), in absence or presence of 0.01μM trabectedin for 15h. The cells were then stimulated in vitro with Brefeldin A (4h, 4μg/ml) and stained with the surface

antibodies described in Supplementary Table S7, after LIVE/DEAD fixable Aqua dye incubation and Fc receptor blocking. Surface-stained cells were further fixed and permeabilized using a Staining Buffer Kit (Miltenyi Biotec) and finally stained with an anti-IFNγ antibody.

RNA extraction, RT-PCR amplification and Quantitative PCR

RNA extraction from sorted myeloid and lymphoid cells was performed using using Mini Kit (QIAGEN, Hilden, Germany). RNA sample quality and quantity checks (QC) were performed using an Agilent RNA 6000 Pico Assay (Agilent Technologies, Santa Clara, CA, USA) at MD Anderson's Sequencing and Non-Coding RNA Program.

Reverse-transcription reaction from 50–200 ng RNA template was done using RevertAid™ H Minus First Strand cDNA Synthesis Kit (Fermentas, Thermo Fisher Scientific) according to the manufacturer's instructions. The sequences of primer pairs specific for each gene sequence (Primm Srl, Milan, Italy and Sigma-Aldrich, St. Louis, MO, USA) were designed with Beacon Designer (Premier Biosoft International; Palo Alto, CA, USA) and NCBI-Primer Designing Tools (Supplementary Table S8).

Real-time PCR was performed using the SYBR® Green PCR Master Mix (Applied Biosystems, Foster City, CA, USA) with forward and reverse primers at a final concentration of 10μM. Each cDNA (2 μl) was used as template; 12.5 μl of 2x SYBR Green PCR Master Mix were mixed with template and primers. The total reaction volume was 25 μl. Three replicates for each cDNA sample were tested. 7900HT Fast Real-Time PCR System (Applied Biosystems) was used, and cycling conditions were 10 min at 95°C (1 cycle); 10 min at 95°C (1 cycle); 15 s at 95°C plus 1 m at 60°C (40 cycles). Data were normalized to β-actin expression.

Mice

All mice were housed and bred in specific pathogen-free animal facilities at San Raffaele Scientific Institute and at the University of Texas M.D. Anderson Cancer Center. Depending on the animal experiment, mice were treated in accordance with the European Union guidelines and with the approval of the San Raffaele Scientific Institute Institutional Ethical Committee (protocols 601 and 726) or with the approval of the Institutional Animal Care and Use Committee of the University of Texas M.D. Anderson Cancer Center (protocol 00001627-RN00) and conducted in accordance with the Animal Welfare Act. Rag2$^{-/-}$γc$^{-/-}$ mice on a BALB/c background were kindly provided by CIEA or purchased by Taconic (Rensselaer, NY, USA), *Eμ-TCL1* transgenic mice on a C57BL/6 background were kindly provided by Dr. Byrd (The Ohio State University, Columbus, OH) and wild-type C57BL/6 mice were supplied by Taconic.

Mice genotyping

Eμ-TCL1 transgenic mice were genotyped for the *hTCL1* transgene by PCR-based screening assay as described previously (35).

Xenograft studies

Eight-week-old male Rag2$^{-/-}\gamma c^{-/-}$ mice were i.v. transplanted (day 0) with 10×10^6 MEC1 cells in 0.1 mL of saline through a 27-gauge needle. In some experiments, mice were i.v. injected with 0.15mg/Kg of trabectedin or with saline (control) weekly. Depending on the experiments mice were monitored once per week for weight and humanely killed at different stages of leukemia. PE, PB, SP and femoral BM were collected and analyzed.

For pre-clinical purposes, Rag2$^{-/-}\gamma c^{-/-}$ mice received s.c. injections of 10×10^6 MEC1 cells in 0.1 mL of saline into the left flank on day 0. Once the mice developed palpable subcutaneous tumors, they were i.v. injected with 0.15mg/kg trabectedin or with saline (control). Mice were monitored once per week for weight and tumor growth (by measuring three perpendicular diameters by a caliper) and killed when the mean subcutaneous tumor volume reached 1000 mm^3 (before reaching clinical signs and symptoms, to avoid unnecessary pain and discomfort according to the ethical guidelines). Measurements were stopped when 75% of the originally treated mice were still surviving. For survival experiments xeno-transplanted mice were i.v. injected with trabectedin on days 11, 18 or with GA101 moAb on days 12, 19 as single agents or in combination settings. For patient-derived xenograft studies, MEC1-transplanted Rag2$^{-/-}\gamma c^{-/-}$ mice were injected i.v. on day 18 with patient-derived CD8$^+$ memory T cells (treated with 0.01μM trabectedin for 16 h in vitro or left untreated) from patients 41–43 (Supplementary Table S2) or with patient derived-monocytes (treated with 0.01μM trabectedin for 16 h in vitro or left untreated) from patients 41–44 (Supplementary Table S2). Mice were humanely killed 5 days after the adoptive transfer. PB, SP, BM were collected and analyzed.

Transgenic studies

Eight-week-old male syngeneic immunocompetent C57BL/6 mice were injected i.p. (day 0) with 10×10^6 cells purified from the spleen of leukemic male *Eμ-TCL1* transgenic mice using the EasySep mouse B-cell enrichment kit (STEMCELL Technologies). The purity of the transplanted CD19$^+$ CD5$^+$ Igκ$^+$ cells was assessed by flow cytometry. Mice were monitored weekly for weight and leukemia development by flow cytometric analysis of PB samples. Mice were i.v. injected with 0.15mg/kg trabectedin every week starting when the frequency of CD19$^+$CD5$^+$ leukemic cells in the PB was 15–20%, compared to C57BL/6 wild-type mice. Mice were monitored weekly for weight and leukemia development by flow cytometric analysis of the PB samples and, depending on the last trabectedin injection, humanely killed at different time points. PE, PB, and organs (SP, LN, femoral BM) were collected and analyzed.

Murine cell preparations and flow cytometry

Peripheral blood (PB), peritoneal exudate (PE), spleen (SP), and femurs were collected from mice, and cells were isolated. Erythrocytes from bone marrow (BM), PE, SP and PB samples were lysed by incubation in ammonium chloride solution (NH_4Cl) lysis buffer (NH_4Cl 0.15 M, $KHCO_3$ 10 mM, Na_2EDTA 0.1 mM, pH 7.2–7.4) for 5 min at room temperature. After blocking of fragment crystallizable (Fc) receptors with Fc block (BD Biosciences) for 10 minutes at room temperature, cells from PB, BM, PE, SP, lymph nodes (LN) were stained with the antibodies (15 min. at 4°C) listed in Supplementary Tables S9–

S10. Depending on the experiments, cells were analyzed with a Beckman Coulter FC500 or with a BD LSRFortessa X-20 flow cytometer. Ten-color flow cytometry phenotype analysis of live myeloid cell singlets and 13-color flow cytometry phenotype analysis of live lymphoid cell singlets were performed using an LSRFortessa X-20. To develop the multi-color flow cytometry panels, we used antibody-capture beads (UltraComp eBeads Invitrogen, Waltham, MA, USA) for single-color compensation controls. A Live/Dead Fixable Aqua Dead Cell Stain Kit (Thermo Fisher Scientific) was used first to gate out dead cells. Further gating adjustments were made based on fluorescence-minus-one (FMO) controls. Absolute cell numbers were obtained by multiplying the percentage of the cells by the total number of splenocytes, mesenteric lymph nodes, peritoneal cells, and BM cells flushed from 1 femur.

Statistics

The statistical analysis of the data was performed using the GraphPad Prism 5.0 Software (San Diego, CA, USA). Data were expressed as means ± standard deviations (SD), and comparison of growth curves or differences between experimental groups were assessed with an unpaired two-tailed Student *t* test (95% confidence interval) and considered statistically significant for *P* values less than 0.05. Survival curves were compared with the use of the log-rank test.

In cell depletion experiments that involved different human myeloid and lymphoid cell types, normality was tested with a Shapiro-Wilk normality test. We applied the *t* test to normally distributed data, otherwise the Mann-Whitney-Wilcoxon test. A box-and-whisker plot (Box plot represents first (lower bound) and third (upper bound) quartiles, whiskers represent 1.5 times the interquartile range) was used to visualize the data. The *y*-axis was plotted on a logarithmic scale for convenience of representation. The analysis and graphical representation were performed in R (version 3.0.1) (http://www.r-project.org/) and the statistical significance was defined as a *P* value less than 0.05.

The outliers at end-point were never excluded. The number of biological and technical replicates for each experiment is detailed in the figure legends. All the experiments were repeated independently and are described in the figures and figure legends. The investigators were not blinded when assessing the analysis of the experimental outcome.

RESULTS

Trabectedin targets both CLL cells and their microenvironment

We first evaluated whether trabectedin affects human primary leukemic cells. As demonstrated previously (26), cytotoxicity studies performed on MEC1 CLL cell line (Supplementary Fig. S1A) and on purified human primary leukemic cells (Fig. 1A, Supplementary Fig. S1B; n=5) revealed that trabectedin has a toxic effect on leukemic B cells in vitro. We selected the lowest trabectedin dose that reduced leukemic B cell viability but did not complete kill them (e.g. 0.01μM, dot line Fig. 1A). The direct cytotoxic activity of trabectedin on CLL cells was confirmed in a flow-cytometry cell-depletion assay (Fig. 1B, empty circles). When unfractionated PBMCs of CLL patients (which contained both

leukemic and normal hematopoietic cells) were treated with 0.01μM trabectedin, we observed depletion of both leukemic B cells and $CD14^+$ myeloid cells (Fig. 1B, black circles). This confirmed the drug's cytotoxicity to mononuclear phagocytes demonstrated in solid tumors (23). Leukemic cell depletion induced by trabectedin increased significantly in the PBMCs as compared to purified leukemic cells, suggesting a role for $CD14^+$ cells and other mononuclear cells (Fig. 1B, Supplementary Table S1).

We next evaluated the effect of trabectedin on monocyte subsets, identified by flow cytometry with a negative exclusion gating strategy (31, 32). CD14 and CD16 expression was used to identify $CD14^+CD16^{++}$ non classical (NC), $CD14^{++}CD16^+$ intermediate (I) and $CD14^{++}CD16^-$ classical (C) monocytes (Fig. 1C, PB; Supplementary Fig. S2A, PBMC). This gating strategy enabled us to better characterize myeloid cells and to avoid nonspecific cell inclusion (31, 32, 36). Monocyte subsets were also screened for the surface expression of HLA-DR protein, because of the demonstrated immunosuppressive activity of HLA-$DR^{low/-}$ classical monocytes in non-Hodgkin lymphoma patients (37) (Supplementary Fig. S2A). Moreover M-MDSCs were analyzed (38, 39). PBMCs from 10 CLL patients were treated with trabectedin: after 24 hours I monocytes and M-MDSCs were depleted, whereas NC and C monocytes (Fig. 1D and 1E, Supplementary Table S2), including their fractions with increased HLA-DR expression, were not depleted (Supplementary Fig. S2B, Supplementary Fig. S3A–B). Trabectedin also increased the absolute number of $CD14^{++}CD16^-$ HLA-DR^+ classical monocytes (Supplementary Fig. S4), high frequency of which have been found to correlate with improved overall survival in metastatic melanoma patients (36). These results led us to conclude that trabectedin affects myeloid cells.

We asked whether trabectedin also affects T lymphocytes. Human naïve, effector (T_{EM}) and central memory (T_{CM}) $CD8^+$ T cells were identified based on the differential surface expression of CD45RO, CD45RA, and CD62L. $CD4^+$ regulatory T lymphocytes expressing CD25 and Foxp3 were also analyzed. In addition to depleting the $CD19^+CD5^+$ leukemic clone, trabectedin reduced $CD4^+$ T regulatory cells. However, trabectedin did not deplete $CD8^+$ T_{EM} and T_{CM} cells (Fig. 1D and 1F and Supplementary Tables S11–S12).

Trabectedin triggers apoptosis of selected immune cells

Based on our findings, we hypothesized that trabectedin directly kills leukemic cells and tumor-supporting immune cells including $CD4^+$ Treg cells and some myeloid cell subtypes (M-MDSCs and I monocytes), and favors the activation of cytotoxic T lymphocytes.

Trabectedin's effects on transcription regulation affect both cancer cells and normal cells of the malignant microenvironment (25), but the effect of the drug on immune cell types from leukemic patients is unexplored. Therefore we analyzed RNA from CLL patient lymphoid and myeloid cell types after 15 h of trabectedin treatment. By means of two independent 4-ways fluorescence-activated cell sorting strategies, we separated myeloid subsets including C, NC, I, M-MDSCs and some of B-T cell types described in Fig. 1D, including leukemic $CD19^+CD5^+$ B cells, $CD8^+$ T_{EM} and T_{CM} cells and Treg cells. For RNA studies $CD4^+$ $CD25^+$ Treg cells were identified and sorted based on low-negative expression of CD127.

We then evaluated by RT-PCR the expression of RNA encoding effector molecules involved in TRAIL-, TNF-, and FAS/FASL-regulated death pathways on cell types depleted by trabectedin (Fig. 1D) including leukemic B cells, regulatory $CD4^+$ T cells, I monocytes and M-MDSCs. As described in Fig. 2, we observed upregulation of molecules involved in TRAIL and TNF pathways including *TRAIL-R2*, *TNFR*1, *BAX*, *BID*, *CASP3* transcripts in all the trabectedin-targeted cells types but not in memory $CD8^+$ T cells (Supplementary Fig. S5). We confirmed the involvement of TRAIL pathway by using a blocking anti-human TRAIL-R2 moAb. In 7/8 samples (Supplementary Fig. S6), the leukemic cell depletion induced by trabectedin was reduced when TRAIL signaling was blocked. Consistent with reported TRAIL-mediated activity of trabectedin in monocytes in solid tumors (23), we confirmed by flow cytometry that trabectedin modulated TRAIL-R2 receptor expression on monocytes and M-MDSCs (Supplementary Fig. S7A). We also observed involvement of TRAIL-mediated cell death pathway in T cells treated with trabectedin (Fig. 2, Supplementary Fig. S6).

Trabectedin has immunomodulatory activity in vitro

We next evaluated the immunomodulatory activity of trabectedin on myeloid and lymphoid cell types. Trabectedin modified RNA expression of proinflammatory cytokines that promote the classical (M1) antitumor activation of macrophages (e.g. *IFNα* and *TNFα*), induce T-cell cytotoxic response (e.g. *IFNα* and *IL12a*), and control B lymphocytes (e.g. *IL6*) (Fig. 3A). Expression of TNFα RNA was also upregulated in M-MDSCs (Fig. 3B).

Expression of RNA encoding *CCL2*, a monocyte chemoattractant, was reduced in C, I and NC monocytes (Fig. 3A, 3C–D), as demonstrated in solid tumors (23, 27). In a different set of CLL patient samples, we confirmed altered production of IL-6, CCL2 and IFNα protein upon 38h trabectedin treatment (Supplementary Fig. S7A–C). Patients 39 and 40 carried a 17p deletion and patient 40 (in red) was in Richter transformation, resistant to ibrutinib and venetoclax (Supplementary Table S2). In some patient PBMC samples, M-MDSCs disappeared after trabectedin treatment.

In Treg cells, trabectedin downregulated *FOXP3*, the transcription factor that modulates the functionality of these cells and abolishes their suppressor activity (Fig. 3E). Unlike leukemic B lymphocytes (26), we did not observe TC-NER and homologous recombination (HR) pathways involvement in the selective targeting of Tregs by trabectedin (Supplementary Fig. S8).

The reduced immunosuppression was accompanied by upregulation of RNA encoding cytolytic factors in $CD8^+$ T_{EM} and T_{CM}, including *IFNγ* and *GRANZYME B* (*GZMB*) (Fig. 3F–G).

Thus, trabectedin enhances the anti-tumor phenotype of monocytes and reprograms the tumor microenvironment towards immune effector T-cell cytotoxicity.

Trabectedin has therapeutic efficacy in CLL mouse models

We verified the *in vivo* antitumor activity of trabectedin in the subcutaneous (s.c.) MEC1-based xenograft model of CLL (Fig. 4A) (40). Treatment significantly reduced subcutaneous

MEC1 tumor growth (Fig. 4B) and induced a significant reduction of $hCD19^+$ leukemic cells in lymphoid tissues, including BM and spleen (SP) (Fig. 4C).

We next performed a time-course experiment in which mice, transplanted intravenously (i.v.) with MEC1 cells, were sacrificed 1 or 10 days after the last of three trabectedin injections (days 27 and 36, respectively) (Fig. 4D). The treatment reduced the leukemic expansion and stabilized the disease in the peripheral blood (PB) and lymphoid tissues, including SP and BM (Fig. 4E–G). Trabectedin also conveyed a survival benefit as both a single agent (Fig. 4H–I p=0.0009, trabectedin vs untreated) and in combination with GA101, a glycoengineered type II CD20 moAb, GA101 (Fig. 4J–K).

Trabectedin affects immune cells of tumor microenvironment *in vivo*

We tested whether trabectedin affected myeloid cells in CLL mouse models, including the xeno- and the TCL1 transgenic- transplantation systems (13). The anti-leukemic effect observed in xeno-transplanted mice sacrificed at day 27, the day after the last injection of the drug (Fig. 4D–G), was associated with a significant reduction of $CD11b^+$ $F4/80^+$ TAMs in the SP and peritoneal exudate (PE), with selective depletion of $MRC1^+$ M2-like pro-tumor TAMs in the PE (Supplementary Fig. S9A–E).

We next used a CLL immunocompetent mouse model, based on the transplantation of leukemic cells purified from the SP of Eμ-*TCL1* transgenic (tg) mice into syngeneic C57/BL6 recipients (13). To evaluate the immune cell dynamics induced by trabectedin and their persistence over time, we performed three sets of experiments in which mice transplanted with leukemic cells from Eμ-*TCL1* tg donors #1, #2, #3 were sacrificed 6, 9 or 13 days after the last trabectedin injection. When donor #1-transplanted mice were treated with trabectedin (starting at day 40) and sacrificed 6 days after the last injection of the drug (day 53), a significant reduction of the leukemic clone in the SP, BM, PE but not in the PB was observed (Supplementary Fig. S10A–D). This reduction was associated with decreased frequencies of $CD11b^+$ $CSF1R^+$ monocytes and $F4/80^+$ macrophages and with selective depletion of $PD\text{-}L1^+$ monocytes and $MRC1^+$ and $PD\text{-}L1^+$ M2-like TAMs in the PE (Supplementary Fig. S10E–I). Among monocytes, we observed a reduction of the $Ly6C^{low}$ cell component expressing PD-L1 in the SP (Supplementary Fig. S10J): such a reduction suppresses T-cell immunity in solid tumors (41). Overall these data are in line with findings on the PD-L1-mediated functional remodeling of monocytes and macrophages in colon and mammary carcinoma (42). We observed a decrease in the whole pool of $Gr1^+$ MDSCs in the PB, BM and SP (Supplementary Fig. S10K–M), an increase of $CD8^+$ T lymphocytes in the BM and SP and an increase of $CD8^+$ memory T cells in the PB and BM (Supplementary Fig. S10N–Q).

To clarify the long-term cell dynamics induced by trabectedin in vivo, we transplanted mice with splenic leukemic cells from TCL1 tg donor mouse #2 or donor mouse #3 and sacrificed them 9 (Fig. 5A, donor #2 recipients) and 13 days (Fig. 5B, donor #3 recipients) after the last trabectedin injection, respectively. In donor #2 recipient mice treated with trabectedin starting on day 25 (Fig. 5A), a significantly lower percentage of leukemic B cells in the PB was observed over time (Fig. 5C). Upon necropsy, comparative analysis of the treated and untreated mice confirmed that in both donor #2 and donor #3 recipient mice, (Fig. 5A–B)

leukemic cell expansion was reduced in the PE, SP, BM, LN (Fig. 5D–G). Trabectedin treatment selectively depleted $CD19^+CD5^+$ leukemic cells expressing PD-L1 in the lymphoid tissues and PE (Supplementary Fig. S11A–C) of donor #3 recipient mice killed 13 days after the last trabectedin injection.

As for the myeloid cells, in mice sacrificed 9 days after the last trabectedin injection (Fig. 5A, donor #2 recipients), numbers of $CSF1R^+$ monocytes (Fig. 5H) and $CD11b^+$ $PD\text{-}L1^+$ (Fig. 5I) monocytes were reduced in the BM, and the $Ly6C^{low}$ subset was the most affected and significantly reduced in the BM and PB (Fig. 5J,K). Conversely, $Ly6C^{high}$ monocytes increased in the spleen of treated mice (Supplementary Fig. S12A, B). In mice sacrificed 13 days after the last trabectedin injection (Fig. 5B, donor #3 recipients), the whole pool of monocytes (Fig. 5L,M), $CD11b^+$ $PD\text{-}L1^+$ monocytes (Fig. 5N,O), and $Ly6C^{low}$ subset (Fig. 5P,Q) were reduced in the BM and PE of treated mice.

As for M-MDSCs and TAMs, we confirmed (Fig. 6A, donor #2 recipients) the reduced frequency of M-MDSCs in the PB, BM, SP, lymph node (LN) and PE (Fig. 6B–F) and that of $MRC1^+$, $PD\text{-}L1^+$ and IAb^{low} pro-tumor TAMs in the BM (Fig. 6G–J). M-MDSCs remained reduced in the SP 13 days after the last trabectedin injection (Fig. 6K–L, donor #3 recipients), as did $CD11b^+$ $F4/80^+$ TAMs and $MRC1^+$, $PD\text{-}L1^+$, and IAb^{low} pro-tumor TAMs in the BM (Fig. 6M–P), SP (Supplementary Fig. S13A–E) and PE (Supplementary Fig. S13F–G).

In treated mice, myeloid cell-targeting by trabectedin was associated with increased frequencies of $CD8^+$, $CD4^+$, $CD8^+$ T_{CM}, $CD4^+$ T_{EM} and T_{CM} in the PB (Supplementary Fig. S14A–E) and decreased frequency of potentially regulatory $CD4^+$ $CD25^+$ Treg cells in the mesenteric lymph nodes (Supplementary Fig. S14F). Thirteen days after last trabectedin treatment (Supplementary Fig. S14G, donor #3 recipients), $CD8^+$ and $CD4^+$ T_{EM} cells were maintained at higher frequencies in circulation (Supplementary Fig. S14H–J), and these frequencies were associated with a significant reduction of $CD4^+$ $CD25^+$ T cells in the PE, SP and LN (Supplementary Fig. S14K–M). These results are in line with the reduction of $PD\text{-}1^+$ $CD8^+$ memory T cells we observed in the BM and LN of trabectedin-treated mice sacrificed 9 (Supplementary Fig. S15A, donor #2 recipients) or 13 (Supplementary Fig. S15B, donor #3 recipients) days after the last treatment (Supplementary Fig. S15C,D).

Trabectedin repairs immune dysfunction of CLL patient-derived cells

To conclusively delineate the direct effect of trabectedin on nonleukemic immune cells, we transplanted patient-derived monocytes or $CD8^+$ memory T cells into leukemic MEC1-transplanted $Rag2^{-/-}\gamma c^{-/-}$ mice. Using fluorescence-activated cell sorting, we separated monocytes (including NC, I and C) from patients 41–44 (Supplementary Table S2) and T cells (including $CD8^+$ T_{EM} and T_{CM}) from patients 41–43 (Supplementary Table S2). After 16 h of in vitro trabectedin treatment (0.01μM), monocytes or $CD8^+$ T cells were adoptively transferred into xeno-transplanted mice (Fig. 7A,B). Compared with mice injected with untreated T cells and monocytes, mice injected with trabectedin-treated T cells and monocytes benefited from significant antileukemic effects in the spleen (Fig. 7C).

The functionality of CLL patient-derived $CD14^+$ monocytes and $CD68^+$ macrophages upon trabectedin was confirmed in vitro in a different set of patient samples by means of a Violet Proliferation Dye (VPD) based assay. The number of not-phagocytosed VPD-labeled $CD14^-$ / VPD^+ MEC1 target cells or $CD68^-$ / VPD^+ MEC1 target cells treated or not with trabectedin was quantified by flow cytometry. In most patient samples tested, trabectedin did not impair the phagocytic ability of monocytes and macrophages (Fig. 7D).

To confirm T-cell functionality upon trabectedin treatment in vitro, $CD8^+$ memory T cells, in the absence or presence of antigen (Ag) stimulation with heated-MEC1 cells, were treated with 0.01μM trabectedin and then assessed for their expression of PD-1 checkpoint markers and ability to produce cytolytic proteins. Upon trabectedin treatment, absolute numbers of total $CD8^+$ and $CD8^+$ T_{EM} cells were not affected (Supplementary Fig. S16A,B), whereas $PD\text{-}1^+$ $CD8^+$ and $PD\text{-}1^+$ T_{EM} cells were reduced significantly (Fig. 7E–H). $CD8^+$ T_{EM} cells retained their capacity for IFNγ and GRANZYME B production in both the presence and absence of trabectedin (Supplementary Fig. S16C,D). Indeed, T cells from CLL patients have increased expression of the PD-1 exhaustion marker but retain their ability to produce cytokines (43). We demonstrated that trabectedin restores T-cell functionality, likely interfering with PD-1 checkpoint molecule.

Overall, these findings indicate that trabectedin inhibits leukemia progression with a cascade of immunomodulatory effects in immune cell types of the malignant microenvironment (Supplementary Fig. S17).

DISCUSSION

In this study, we demonstrated that in CLL trabectedin interfered with leukemic cells and nonleukemic myeloid and lymphoid cells of the microenvironment.

In vitro, trabectedin was directly cytotoxic to human primary leukemic cells. It upregulated mRNAs for several cell death TRAIL and TNF pathway elements like *CASP3* (supporting the caspase 3 activity seen in CLL, ref. 26), while downregulating the mRNA for anti-apoptotic *MCL1*.

Trabectedin depleted selected human myeloid cell subtypes by rapidly engaging *CASPASES* and other cell death pathway elements, corroborating previous findings with *CASP8* (23). The murine counterpart of human $CD16^+$ monocyte subsets is represented by $Ly6C^{low}$ monocytes (44) which were depleted by trabectedin in our CLL mouse studies, in a T cell-independent manner. In mice, trabectedin depleted $Ly6C^{low}$ monocytes expressing PD-L1, which inhibits T cell proliferation and cytotoxic potential in solid tumors (41). In contrast, trabectedin has a selective activity on $Ly6C^{high}$ monocytes in murine fibrosarcoma (23), implicating a different leukemia-dependent cell mechanism (45). Patient-derived xenograft and *in vitro* phagocytosis studies showed that trabectedin enhanced antitumor functionality of monocytes and macrophages. These trabectedin-dependent effector cell mechanisms are reminiscent of the immunomodulatory activity of lenalidomide, a regulator of T-cell and macrophage function in CLL (33, 46).

Trabectedin had selective activity against human and mouse M-MDSCs, which inhibit T-cell activity (39) and limit antitumor activity through immunosuppression in CLL (14). In human *in vitro* studies and *in vivo* mouse models, targeting M-MDSCs was associated with reduced expression of transcription factor *FOXP3* mRNA and the depletion of immunosuppressive Treg cells, which often accumulate in CLL patients and are linked to worse prognosis and advanced disease (47). Trabectedin can break the immunosuppressive biological crosstalk among CLL cells, MDSCs, and Treg cells.

Consistent with data in fibrosarcoma (23), long-term targeting of murine M2-like pro-tumor TAMs was another determinant of *in vivo* trabectedin efficacy in CLL mouse models.

Effects other than tumor-associated myeloid cell depletion were involved in the antitumor activity of trabectedin, including downregulation of chemokine *CCL2* RNA and protein expression in all monocyte subtypes. The CCL2/CCR2 axis is involved in the recruitment of myeloid cells at the tumor sites and several antitumor strategies interfere with this axis (48). Another effect of trabectedin, was the rapid increase in mRNA expression of proinflammatory cytokines that promote the classical M1 antitumor activation of macrophages, inducing T-cell responses and interfering with B cell activity (49). TNFα, IFNα, IL12a, and IL6 RNA and protein were differentially expressed by human classical monocytes and M-MDSCs. Cytokines including IFNα might be induced as a byproduct of the DNA repair mechanisms (50). These transcriptional changes correlated with the induction of mRNA transcripts for *IFNy* and *GZMB* cytolytic factors in human memory T lymphocytes. Supporting our *in vitro* findings in human PBMCs, we observed induction of circulating memory $CD4^+$ and $CD8^+$ T cells in the TCL1 tg immunocompetent mouse system. Trabectedin effects on T cells were consistent with osteosarcoma showing that recruitment and expansion of adaptive T cells were induced by trabectedin (28). However, in our immunocompetent mouse system, trabectedin interfered with the PD-1/PD-L1 axis in the lymphoid tissues by reducing CLL cells as well as monocytes/macrophages expressing PD-L1, and also memory $CD8^+$ T cells expressing PD-1. Unlike for osteosarcoma and pancreatic adenocarcinoma (28, 51), in primary CLL patient cells, trabectedin reduced PD-1 and restored $CD8^+$ T cell antitumor function. Alterations in DNA damage response and repair genes are associated with response to PD-1/PD-L1 blockade in patients with metastatic solid tumors (52). In addition, the downmodulation of PD-L1 we observed on myeloid cells is in line with evidence on the role of PD-1/PD-L1 checkpoint in monocyte/macrophage remodeling (42) and indicates that trabectedin has immunomodulatory activity.

Trabectedin, besides having a cytotoxic effect in leukemic cells, has immunomodulatory activity on several cell types of the microenvironment. Our findings suggest a therapeutic strategy in which one drug hits both the leukemic cell compartment and the protumor microenvironment, repairing CLL immune dysfunction. Future studies should aim to clarify the molecular mechanisms by which trabectedin functions in the distinct immune cell types.

Supplementary Material

Refer to Web version on PubMed Central for supplementary material.

ACKNOWLEDGEMENTS

Eμ-TCL1 transgenic mice were from J. Byrd and C.M. Croce (Columbus, OH). Rag2$^{-/-}\gamma c^{-/-}$ mice on BALB/c background were provided by CIEA (Kawasaki, Japan) and Taconic. We thank PharmaMar, S.A. for providing trabectedin., the Department of Scientific Publications, MD Anderson Cancer Center, for reviewing the manuscript and providing constructive comments. Figures were produced using Servier Medical Art: www.servier.com.

Financial support: This study was supported by the CLL Global Research Foundation (to M.T.S.B and V.G.), The UT MD Anderson Cancer Center Moon Shots Program (to M.T.S.B., to V.G and to M.J.K.), Roche (to M.T.S.B.), NCI P30CA016672 (to The South Campus Flow Cytometry & Cell Sorting Core MD Anderson Cancer Center), and Program Molecular Clinical Oncology-5 per mille number 9965 (to F.C.-C.) Associazione Italiana per la Ricerca sul Cancro AIRC (Italy).

REFERENCES

1. Ahn IE, Underbayev C, Albitar A, Herman SE, Tian X, Maric I, et al. Clonal evolution leading to ibrutinib resistance in chronic lymphocytic leukemia. Blood. 2017;129(11):1469–79. doi: 10.1182/blood-2016-06-719294. [PubMed: 28049639]
2. Furman RR, Cheng S, Lu P, Setty M, Perez AR, Guo A, et al. Ibrutinib resistance in chronic lymphocytic leukemia. N Engl J Med. 2014;370(24):2352–4. doi: 10.1056/NEJMc1402716. [PubMed: 24869597]
3. Blombery P, Anderson MA, Gong JN, Thijssen R, Birkinshaw RW, Thompson ER, et al. Acquisition of the recurrent Gly101Val mutation in BCL2 confers resistance to venetoclax in patients with progressive chronic lymphocytic leukemia. Cancer Discov. 2018. doi: 10.1158/2159-8290.CD-18-1119.
4. Varughese T, Taur Y, Cohen N, Palomba ML, Seo SK, Hohl TM, et al. Serious Infections in Patients Receiving Ibrutinib for Treatment of Lymphoid Malignancies. Clin Infect Dis. 2018. doi: 10.1093/cid/ciy175.
5. Lionakis MS, Dunleavy K, Roschewski M, Widemann BC, Butman JA, Schmitz R, et al. Inhibition of B Cell Receptor Signaling by Ibrutinib in Primary CNS Lymphoma. Cancer Cell. 2017;31(6):833–43 e5. doi: 10.1016/j.ccell.2017.04.012. [PubMed: 28552327]
6. Kavanagh JJ, Krakoff IH, Bodey GP. Phase I study of fludarabine (2-fluoro-ara-AMP). Eur J Cancer Clin Oncol. 1985;21(9):1009–11. [PubMed: 2415365]
7. Keating MJ, Kantarjian H, Talpaz M, Redman J, Koller C, Barlogie B, et al. Fludarabine: a new agent with major activity against chronic lymphocytic leukemia. Blood. 1989;74(1):19–25. [PubMed: 2473795]
8. Keating MJ. Fludarabine phosphate in the treatment of chronic lymphocytic leukemia. Semin Oncol. 1990;17(5 Suppl 8):49–62.
9. Robertson LE, O'Brien S, Kantarjian H, Koller C, Beran M, Andreeff M, et al. A 3-day schedule of fludarabine in previously treated chronic lymphocytic leukemia. Leukemia. 1995;9(9):1444–9. [PubMed: 7658710]
10. McLaughlin P, Robertson LE, Keating MJ. Fludarabine phosphate in lymphoma: an important new therapeutic agent. Cancer Treat Res. 1996;85:3–14. [PubMed: 9043771]
11. Kipps TJ, Stevenson FK, Wu CJ, Croce CM, Packham G, Wierda WG, et al. Chronic lymphocytic leukaemia. Nat Rev Dis Primers. 2017;3:17008. doi: 10.1038/nrdp.2017.8. [PubMed: 28179635]
12. D'Arena G, Laurenti L, Minervini MM, Deaglio S, Bonello L, De Martino L, et al. Regulatory T-cell number is increased in chronic lymphocytic leukemia patients and correlates with progressive disease. Leuk Res. 2011;35(3):363–8. doi: 10.1016/j.leukres.2010.08.010. [PubMed: 20880586]
13. Galletti G, Scielzo C, Barbaglio F, Rodriguez TV, Riba M, Lazarevic D, et al. Targeting Macrophages Sensitizes Chronic Lymphocytic Leukemia to Apoptosis and Inhibits Disease Progression. Cell Rep. 2016;14(7):1748–60. doi: 10.1016/j.celrep.2016.01.042. [PubMed: 26876171]
14. Jitschin R, Braun M, Buttner M, Dettmer-Wilde K, Bricks J, Berger J, et al. CLL-cells induce IDOhi CD14+HLA-DRlo myeloid-derived suppressor cells that inhibit T-cell responses and promote TRegs. Blood. 2014;124(5):750–60. doi: 10.1182/blood-2013-12-546416. [PubMed: 24850760]

15. Riches JC, Gribben JG. Immunomodulation and immune reconstitution in chronic lymphocytic leukemia. Semin Hematol. 2014;51(3):228–34. doi: 10.1053/j.seminhematol.2014.05.006. [PubMed: 25048786]

16. Fraietta JA, Lacey SF, Orlando EJ, Pruteanu-Malinici I, Gohil M, Lundh S, et al. Determinants of response and resistance to CD19 chimeric antigen receptor (CAR) T cell therapy of chronic lymphocytic leukemia. Nat Med. 2018;24(5):563–71. doi: 10.1038/s41591-018-0010-1. [PubMed: 29713085]

17. Jak M, Mous R, Remmerswaal EB, Spijker R, Jaspers A, Yague A, et al. Enhanced formation and survival of CD4+ CD25hi Foxp3+ T-cells in chronic lymphocytic leukemia. Leuk Lymphoma. 2009;50(5):788–801. doi: 10.1080/10428190902803677. [PubMed: 19452318]

18. Bagnara D, Kaufman MS, Calissano C, Marsilio S, Patten PE, Simone R, et al. A novel adoptive transfer model of chronic lymphocytic leukemia suggests a key role for T lymphocytes in the disease. Blood. 2011;117(20):5463–72. doi: 10.1182/blood-2010-12-324210. [PubMed: 21385850]

19. Burger JA, Tsukada N, Burger M, Zvaifler NJ, Dell'Aquila M, Kipps TJ. Blood-derived nurse-like cells protect chronic lymphocytic leukemia B cells from spontaneous apoptosis through stromal cell-derived factor-1. Blood. 2000;96(8):2655–63. [PubMed: 11023495]

20. Filip AA, Cisel B, Koczkodaj D, Wasik-Szczepanek E, Piersiak T, Dmoszynska A. Circulating microenvironment of CLL: are nurse-like cells related to tumor-associated macrophages? Blood Cells Mol Dis. 2013;50(4):263–70. doi: 10.1016/j.bcmd.2012.12.003. [PubMed: 23313631]

21. McGovern Y, Zhou CD, Jones RL. Systemic Therapy in Metastatic or Unresectable Well-Differentiated/Dedifferentiated Liposarcoma. Front Oncol. 2017;7:292. doi: 10.3389/fonc.2017.00292. [PubMed: 29250486]

22. Teplinsky E, Herzog TJ. The efficacy of trabectedin in treating ovarian cancer. Expert Opin Pharmacother. 2017;18(3):313–23. doi: 10.1080/14656566.2017.1285282. [PubMed: 28140689]

23. Germano G, Frapolli R, Belgiovine C, Anselmo A, Pesce S, Liguori M, et al. Role of macrophage targeting in the antitumor activity of trabectedin. Cancer Cell. 2013;23(2):249–62. doi: 10.1016/j.ccr.2013.01.008. [PubMed: 23410977]

24. Erba E, Bergamaschi D, Bassano L, Damia G, Ronzoni S, Faircloth GT, et al. Ecteinascidin-743 (ET-743), a natural marine compound, with a unique mechanism of action. Eur J Cancer. 2001;37(1):97–105. [PubMed: 11165136]

25. D'Incalci M, Galmarini CM. A review of trabectedin (ET-743): a unique mechanism of action. Mol Cancer Ther. 2010;9(8):2157–63. doi: 10.1158/1535-7163.MCT-10-0263. [PubMed: 20647340]

26. Lohmann G, Vasyutina E, Bloehdorn J, Reinart N, Schneider JI, Babu V, et al. Targeting transcription-coupled nucleotide excision repair overcomes resistance in chronic lymphocytic leukemia. Leukemia. 2017;31(5):1177–86. doi: 10.1038/leu.2016.294. [PubMed: 27773933]

27. Belgiovine C, Bello E, Liguori M, Craparotta I, Mannarino L, Paracchini L, et al. Lurbinectedin reduces tumour-associated macrophages and the inflammatory tumour microenvironment in preclinical models. Br J Cancer. 2017;117(5):628–38. doi: 10.1038/bjc.2017.205. [PubMed: 28683469]

28. Ratti C, Botti L, Cancila V, Galvan S, Torselli I, Garofalo C, et al. Trabectedin Overrides Osteosarcoma Differentiative Block and Reprograms the Tumor Immune Environment Enabling Effective Combination with Immune Checkpoint Inhibitors. Clin Cancer Res. 2017;23(17):5149–61. doi: 10.1158/1078-0432.CCR-16-3186. [PubMed: 28600479]

29. Allavena P, Signorelli M, Chieppa M, Erba E, Bianchi G, Marchesi F, et al. Anti-inflammatory properties of the novel antitumor agent yondelis (trabectedin): inhibition of macrophage differentiation and cytokine production. Cancer Res. 2005;65(7):2964–71. doi: 10.1158/0008-5472.CAN-04-4037. [PubMed: 15805300]

30. Mossner E, Brunker P, Moser S, Puntener U, Schmidt C, Herter S, et al. Increasing the efficacy of CD20 antibody therapy through the engineering of a new type II anti-CD20 antibody with enhanced direct and immune effector cell-mediated B-cell cytotoxicity. Blood. 2010;115(22):4393–402. doi: 10.1182/blood-2009-06-225979. [PubMed: 20194898]

31. Bertilaccio MTS, Zhang R, Banerjee P, Gandhi V. In Vitro Assay to Study CLL and Monocyte Interactions. Methods Mol Biol. 2019;1881:113–9. doi: 10.1007/978-1-4939-8876-1_9. [PubMed: 30350201]
32. Abeles RD, McPhail MJ, Sowter D, Antoniades CG, Vergis N, Vijay GK, et al. CD14, CD16 and HLA-DR reliably identifies human monocytes and their subsets in the context of pathologically reduced HLA-DR expression by CD14(hi) /CD16(neg) monocytes: Expansion of CD14(hi) / CD16(pos) and contraction of CD14(lo) /CD16(pos) monocytes in acute liver failure. Cytometry A. 2012;81(10):823–34. doi: 10.1002/cyto.a.22104. [PubMed: 22837127]
33. Busch L, Mougiakakos D, Buttner-Herold M, Muller MJ, Volmer DA, Bach C, et al. Lenalidomide enhances MOR202-dependent macrophage-mediated effector functions via the vitamin D pathway. Leukemia. 2018. doi: 10.1038/s41375-018-0114-0.
34. Adkins I, Sadilkova L, Hradilova N, Tomala J, Kovar M, Spisek R. Severe, but not mild heat-shock treatment induces immunogenic cell death in cancer cells. Oncoimmunology. 2017;6(5):e1311433. doi: 10.1080/2162402X.2017.1311433. [PubMed: 28638734]
35. Bertilaccio MT, Simonetti G, Dagklis A, Rocchi M, Rodriguez TV, Apollonio B, et al. Lack of TIR8/SIGIRR triggers progression of chronic lymphocytic leukemia in mouse models. Blood. 2011;118(3):660–9. doi: 10.1182/blood-2011-01-329870. [PubMed: 21652674]
36. Krieg C, Nowicka M, Guglietta S, Schindler S, Hartmann FJ, Weber LM, et al. High-dimensional single-cell analysis predicts response to anti-PD-1 immunotherapy. Nat Med. 2018;24(2):144–53. doi: 10.1038/nm.4466. [PubMed: 29309059]
37. Xiu B, Lin Y, Grote DM, Ziesmer SC, Gustafson MP, Maas ML, et al. IL-10 induces the development of immunosuppressive CD14(+)HLA-DR(low/-) monocytes in B-cell non-Hodgkin lymphoma. Blood Cancer J. 2015;5:e328. doi: 10.1038/bcj.2015.56. [PubMed: 26230952]
38. Bronte V, Brandau S, Chen SH, Colombo MP, Frey AB, Greten TF, et al. Recommendations for myeloid-derived suppressor cell nomenclature and characterization standards. Nat Commun. 2016;7:12150. doi: 10.1038/ncomms12150. [PubMed: 27381735]
39. Kumar V, Patel S, Tcyganov E, Gabrilovich DI. The Nature of Myeloid-Derived Suppressor Cells in the Tumor Microenvironment. Trends Immunol. 2016;37(3):208–20. doi: 10.1016/j.it.2016.01.004. [PubMed: 26858199]
40. Bertilaccio MT, Scielzo C, Simonetti G, Ponzoni M, Apollonio B, Fazi C, et al. A novel Rag2−/−gammac−/−-xenograft model of human CLL. Blood. 2010;115(8):1605–9. doi: 10.1182/blood-2009-05-223586. [PubMed: 20018917]
41. Kuang DM, Zhao Q, Peng C, Xu J, Zhang JP, Wu C, et al. Activated monocytes in peritumoral stroma of hepatocellular carcinoma foster immune privilege and disease progression through PD-L1. J Exp Med. 2009;206(6):1327–37. doi: 10.1084/jem.20082173. [PubMed: 19451266]
42. Xiong H, Mittman S, Rodriguez R, Moskalenko M, Pacheco-Sanchez P, Yang Y, et al. Anti-PD-L1 treatment results in functional remodeling of the macrophage compartment. Cancer Res. 2019. doi: 10.1158/0008-5472.CAN-18-3208.
43. Riches JC, Davies JK, McClanahan F, Fatah R, Iqbal S, Agrawal S, et al. T cells from CLL patients exhibit features of T-cell exhaustion but retain capacity for cytokine production. Blood. 2013;121(9):1612–21. doi: 10.1182/blood-2012-09-457531. [PubMed: 23247726]
44. Ingersoll MA, Spanbroek R, Lottaz C, Gautier EL, Frankenberger M, Hoffmann R, et al. Comparison of gene expression profiles between human and mouse monocyte subsets. Blood. 2010;115(3):e10–9. doi: 10.1182/blood-2009-07-235028. [PubMed: 19965649]
45. Hanna BS, McClanahan F, Yazdanparast H, Zaborsky N, Kalter V, Rossner PM, et al. Depletion of CLL-associated patrolling monocytes and macrophages controls disease development and repairs immune dysfunction in vivo. Leukemia. 2016;30(3):570–9. doi: 10.1038/leu.2015.305. [PubMed: 26522085]
46. Ramsay AG, Johnson AJ, Lee AM, Gorgun G, Le Dieu R, Blum W, et al. Chronic lymphocytic leukemia T cells show impaired immunological synapse formation that can be reversed with an immunomodulating drug. J Clin Invest. 2008;118(7):2427–37. doi: 10.1172/JCI35017. [PubMed: 18551193]

47. Lad DP, Varma S, Varma N, Sachdeva MU, Bose P, Malhotra P. Regulatory T-cells in B-cell chronic lymphocytic leukemia: their role in disease progression and autoimmune cytopenias. Leuk Lymphoma. 2013;54(5):1012–9. doi: 10.3109/10428194.2012.728287. [PubMed: 23009220]

48. Majety M, Runza V, Lehmann C, Hoves S, Ries CH. A drug development perspective on targeting tumor-associated myeloid cells. FEBS J. 2018;285(4):763–76. doi: 10.1111/febs.14277. [PubMed: 28941174]

49. Park SH, Kang K, Giannopoulou E, Qiao Y, Kang K, Kim G, et al. Type I interferons and the cytokine TNF cooperatively reprogram the macrophage epigenome to promote inflammatory activation. Nat Immunol. 2017;18(10):1104–16. doi: 10.1038/ni.3818. [PubMed: 28825701]

50. Brzostek-Racine S, Gordon C, Van Scoy S, Reich NC. The DNA damage response induces IFN. J Immunol. 2011;187(10):5336–45. doi: 10.4049/jimmunol.1100040. [PubMed: 22013119]

51. Borgoni S, Iannello A, Cutrupi S, Allavena P, D'Incalci M, Novelli F, et al. Depletion of tumor-associated macrophages switches the epigenetic profile of pancreatic cancer infiltrating T cells and restores their anti-tumor phenotype. Oncoimmunology. 2018;7(2):e1393596. doi: 10.1080/2162402X.2017.1393596. [PubMed: 29308326]

52. Keenan TE, Burke KP, Van Allen EM. Genomic correlates of response to immune checkpoint blockade. Nat Med. 2019;25(3):389–402. doi: 10.1038/s41591-019-0382-x. [PubMed: 30842677]

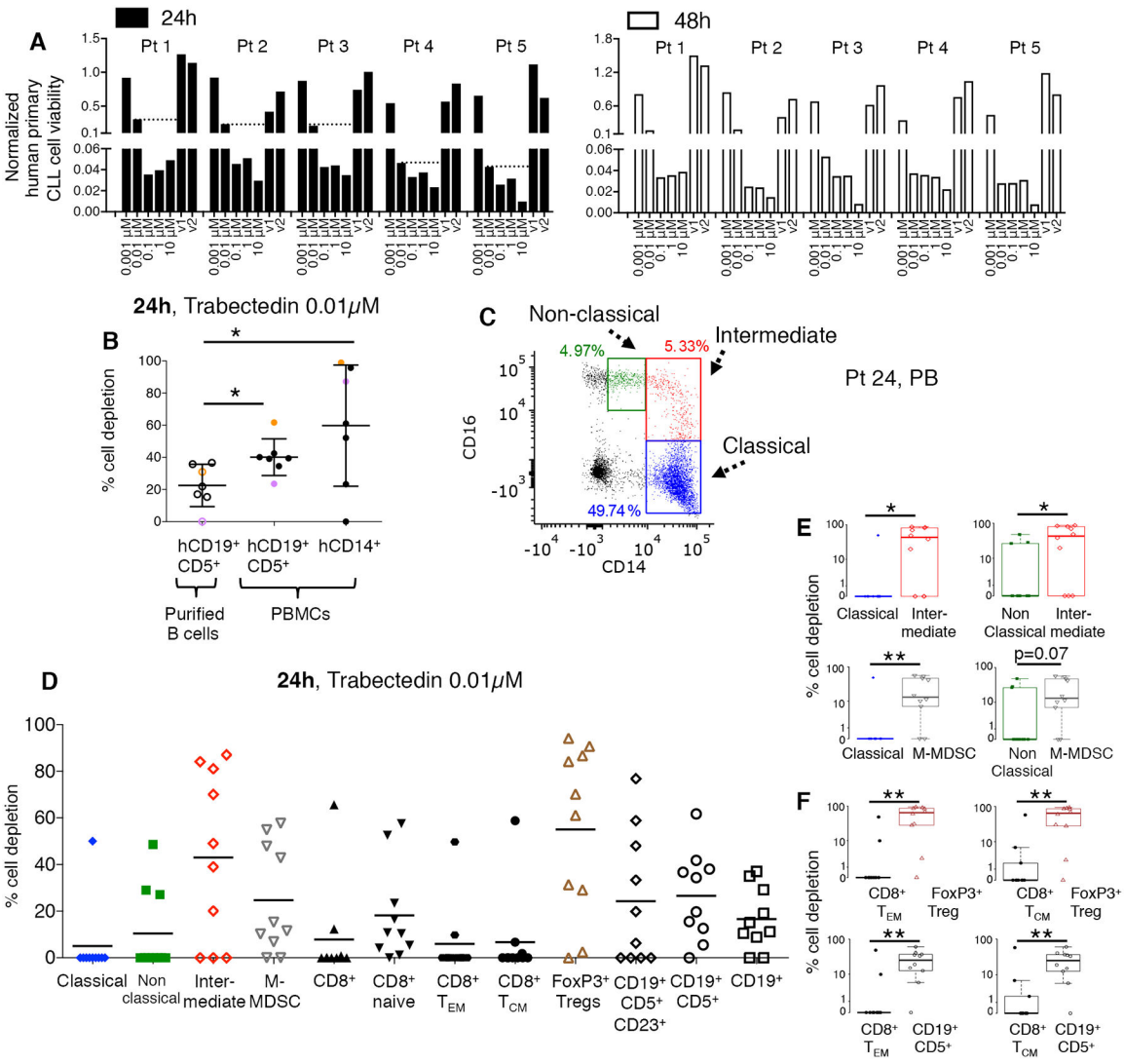

Figure 1. Trabectedin depletes selected human primary lymphoid and myeloid cells.

(**A**) Human primary CLL cells obtained from CLL patients (n=5, patients 1–5, Supplementary Table S1) were incubated with increasing concentrations of trabectedin (or with vehicle (DMSO v1, v2) and subjected to a luminescent assay at 24 and 48 hours to assess the cells' sensitivity to the drug. Cell viability of each sample was normalized to its control. Dot lines indicate CLL cell viability at 0.01μM trabectedin. (**B**) The percentage of depletion of hCD19^{+} CD5^{+} cells (plated alone, empty circles; plated with total PBMCs, black circles) and hCD14^{+} cells (plated with total PBMCs, black circles) after 24h of treatment (n=7, patients 6–12, Supplementary Table S1) with 0.01μM of trabectedin was analyzed by flow cytometry Purple and orange dots identify two representative CLL patients. *p<0.05, Student's t test. (**C**) Monocytes were identified as CD14^{+} CD16^{++} non classical (green), CD14^{++} CD16^{+} intermediate (red) and CD14^{++} CD16^{-} classical (blue) subsets. A representative PB sample from CLL patient 24 (Supplementary Table S2) is described. (**D**) Classical monocytes, non classical monocytes, intermediate monocytes, and hCD14^{+}HLADR$^{low/-}$ M-MDSCs cell depletion and CD8^{+} T cell, naïve T cell, hCD8^{+} T_{CM},

hCD8$^+$ T_{EM}, regulatory hCD4$^+$CD25$^+$Foxp3$^+$ Treg, hCD19$^+$, hCD19$^+$CD5$^+$, and hCD19$^+$CD5$^+$CD23$^+$ lymphoid cell depletion (n=10; patients 20–26, 45, 48, and 49, Supplementary Table S2) after 24 h of treatment with 0.01μM of trabectedin were analyzed by multi-color flow cytometry and calculated by the formula described in the Methods. The statistical analysis is described in Supplementary Tables S11 and S12: (**E**-**F**) An alternate presentation of the distribution of data from **D** showing selected paired-cell type comparisons is depicted by box and whisker plots. P value is given by Mann-Whitney-Wilcoxon test, *$p < 0.05$, **$p < 0.01$.

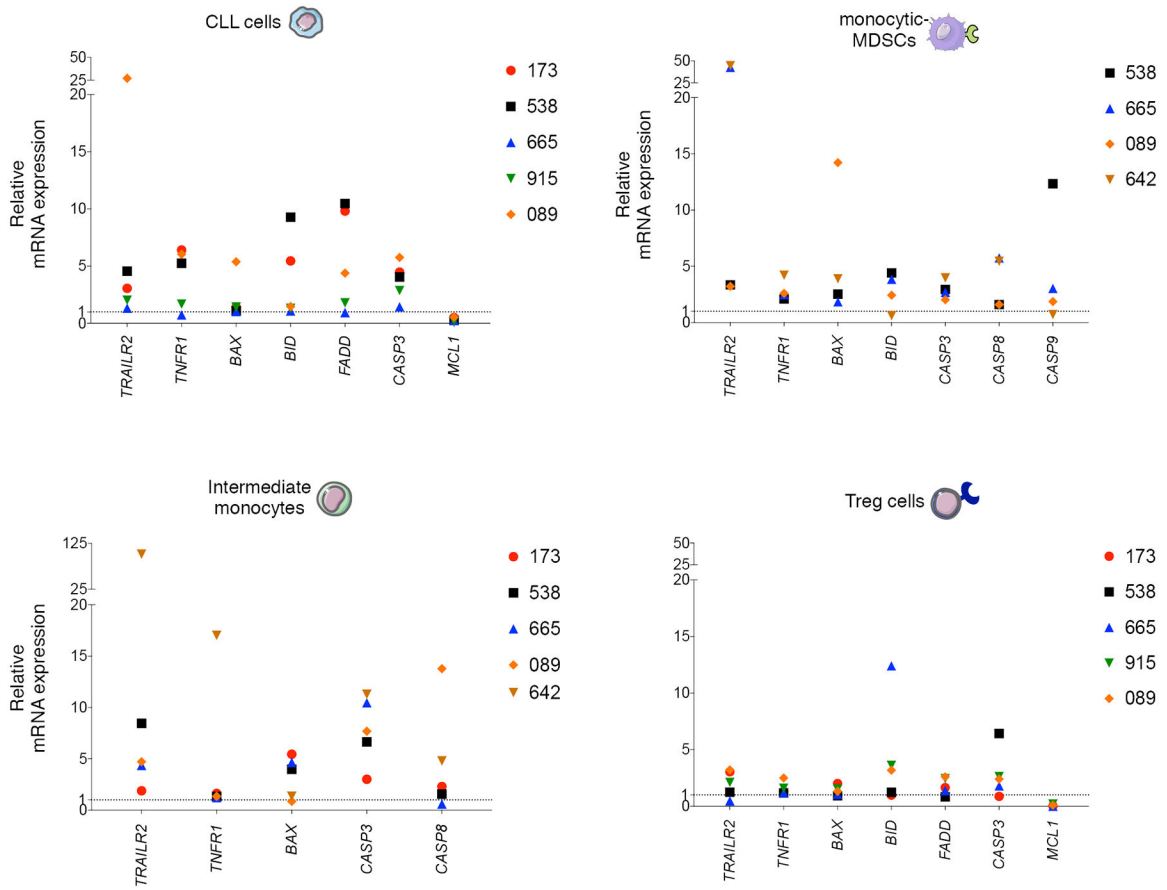

Figure 2. Trabectedin-induced cell death mechanisms in selected primary lymphoid and myeloid cells from CLL patients.

Relative mRNA expression of *TRAILR2*, *TNFR1*, *BAX*, *BID*, *FADD*, *CASP 3*, *CASP 8*, *CASP 9*, and *MCL1* in hCD19^{+}CD5^{+} human primary CLL cells, CD14^{+}HLADR$^{low/-}$ M-MDSCs, intermediate monocytes and CD4^{+}CD25^{+}CD127$^{low/-}$ Tregs separated by FACS from PBMCs (n=6, patients 173, 538, 665, 915, 089, 642, Supplementary Table S2) and plated in 6-well plates alone or with 0.01 μM of trabectedin for 15 h. Three technical replicates were analyzed for each sample. Data were normalized to β-actin expression. Gene expression was determined by calculating the difference (ΔCt) between the threshold cycle (Ct) of each gene and that of the reference gene and was expressed as the mean of 3 replicates ± SEM. Then the relative quantification values were calculated as the fold change expression of the gene of interest over its expression in the selected cell type reference sample, i.e., the untreated sample (considered as the calibrator sample), by the formula $2^{-\Delta\Delta Ct}$. Finally the treated sample relative mRNA expression was normalized to the vehicle. Samples with undetermined Ct values are not included.

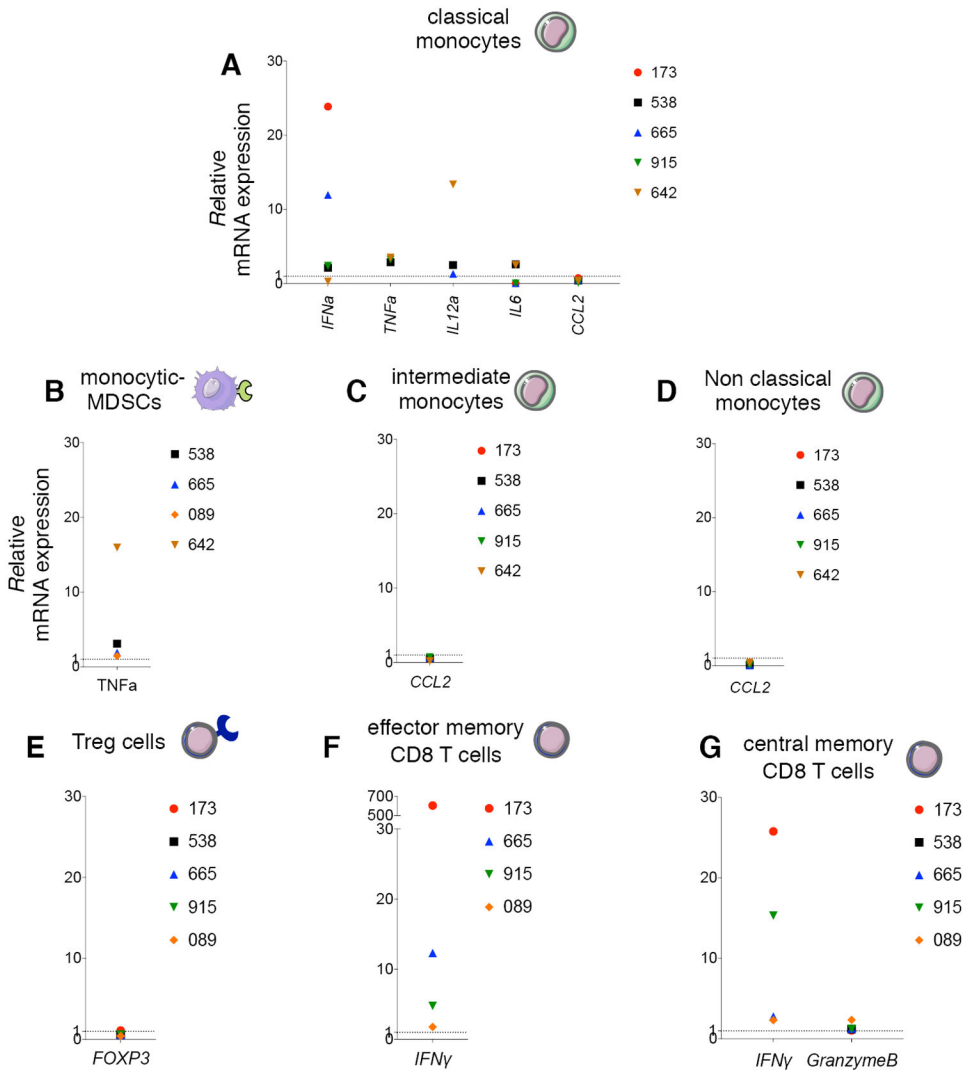

Figure 3. Immunomodulatory activity of trabectedin in human myeloid and lymphoid cell types in CLL in vitro

(**A**) Relative mRNA expression of *IFNα*, *TNFα*, *IL12a*, *IL6, CCL2* in classical monocytes; (**B**) *TNFα* in M-MDSCs; (**C**) *CCL2* in intermediate monocytes; (**D**) *CCL2* in non classical monocytes; (**E**) *FOXP3* on $CD4^{+}CD25^{+}CD127^{low/-}$ Tregs; (**F**) *IFNγ* in $hCD8^{+}$ T_{EM};(**G**) *IFNγ and GZMB* in $hCD8^{+}$ T_{CM}. All cells were separated by FACS from CLL patient PBMCs (n=6, patients 173, 538, 665, 915, 089, 642 Supplementary Table S2), and plated in 6-well plates alone or with 0.01 μM of trabectedin for 15 h. Three technical replicates were analyzed for each sample. Data were normalized to β-actin expression. The gene expression was determined by calculating the difference (ΔCt) between the threshold cycle (Ct) of each gene and that of the reference gene and was expressed as the mean of 3 replicates± SEM. Then the relative quantification values were calculated as the fold change expression of the gene of interest over its expression in the selected cell type reference sample, i.e., the untreated sample (considered as the calibrator sample), by the formula $2^{-\Delta\Delta Ct}$. Finally the treated sample relative mRNA expression was normalized to the vehicle. Samples with undetermined Ct values are not included.

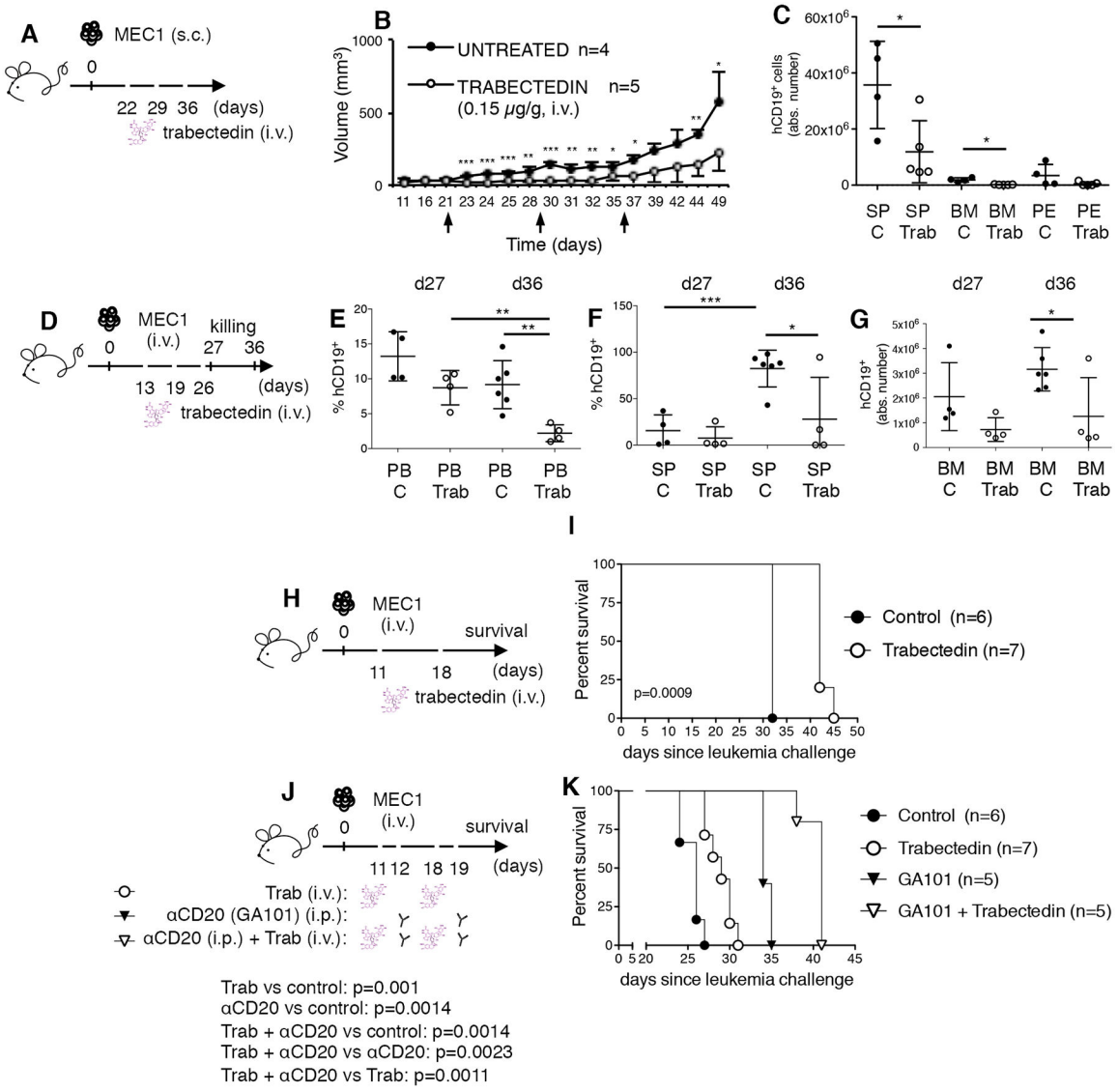

Figure 4. Anti-leukemic effect and survival benefit of trabectedin in the CLL xeno-transplantation systems

(**A-B-C**) Rag2$^{-/-}\gamma c^{-/-}$ mice subcutaneously (s.c.) transplanted with MEC1 cells (day 0) received weekly intravenous (i.v.) injections of 0.15mg/kg of trabectedin on days 22, 29, and 36 (n=5, white circles) or were left untreated (n=4, black circles). (**B**) Tumor size was evaluated as described in the Methods. Statistically significant differences were calculated using the Student *t* test, *p < 0.05, **p < 0.01, ***p < 0.001. (**C**) The mean value ± SD of the relative contribution of CD19$^+$ cells in spleen (SP), bone marrow (BM) and peritoneal exudate (PE) is shown in graph. Statistical analysis: *p < 0.05, Student's t test. (**D-E-F-G**) Rag2$^{-/-}\gamma c^{-/-}$ mice intravenously transplanted with MEC1 cells (day 0) were left uninjected (n=10, black circles) or i.v. treated (days +13, +19, +26) with 0.15mg/kg of trabectedin (n=8, white circles) and killed at day 27 and 36. (**E**) The mean value ± SD of the percentage of hCD19$^+$ in the PB, (**F**) the mean value of the absolute number of hCD19$^+$in the SP and (**G**) the mean value ± SD of the absolute number of hCD19$^+$in the BM are shown in graphs.

*p < 0.05, **p < 0.01, ***p < 0.001, Student's t test. (**H**-**I**) Rag2$^{-/-}\gamma c^{-/-}$ mice intravenously transplanted with MEC1 cells (day 0) were left untreated (n=6, black circles) or treated i.v. (days +11, +18) with 0.15mg/kg of trabectedin (n=7, white circles) and monitored for survival. (**I**) Kaplan-Meier survival curve is represented, statistical analysis was performed using Log-Rank test. ***p < 0.001. (**J**-**K**) Rag2$^{-/-}\gamma c^{-/-}$ mice i.v. transplanted with MEC1 cells were left untreated (n=6, black circles) or treated with: 0.15mg/Kg i.v. of trabectedin (n=7, white circles; day +11, +18); or 30mg/Kg i.p. of anti-CD20 GA101 (n=5, black triangles; day +12, +19); or 0.15mg/Kg i.v. of trabectedin (day +11, +18) + 30mg/Kg i.p. of anti-CD20 GA101 (day +12, +19) (n=5, white triangles) and monitored for survival. (K) Kaplan-Meier survival curve is represented, statistical analysis was performed using Log-Rank test. trabectedin vs control: p=0.001; αCD20 vs control: p=0.0014; trabectedin + αCD20 vs control: p=0.0014; trabectedin + αCD20 vs trabectedin: p=0.0011.

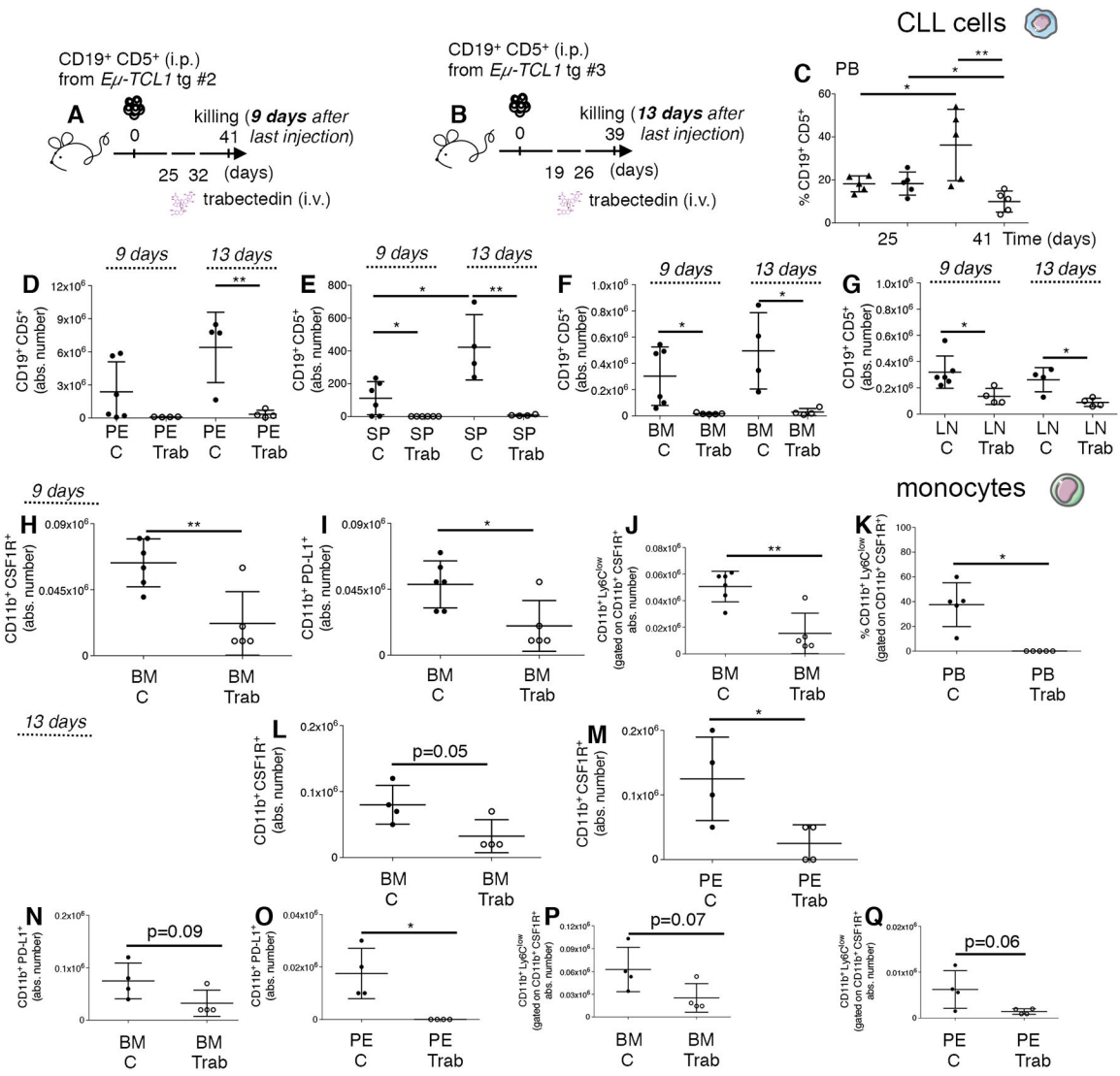

Figure 5. Long-term impact of trabectedin on leukemic cells and on monocytes in the TCL1 tg transplantation system

(**A**) C57BL/6 mice intraperitoneally (i.p.) transplanted with leukemic B cells from *Eμ-TCL1* transgenic mouse donor #2, left untreated (n=6, black circles) or treated (day +25, +32) with 0.15mg/Kg i.v. of trabectedin (n=5, white circles) were killed on day 41 (9 days after the last injection of trabectedin) and analyzed by flow cytometry. (**B**) C57BL/6 mice i.p. transplanted with leukemic B cells from *Eμ-TCL1* transgenic mouse donor #3, left untreated (n=4, black circles) or treated (day +19, +26) with 0.15mg/Kg i.v. of trabectedin (n=4, white circles) were killed on day 39 (13 days after the last injection of trabectedin) and analyzed by flow cytometry. (**C**) The mean value ± SD of the relative contribution of $CD19^+$ $CD5^+$ cells to the whole B cell pool over time in PB of mice described in (A) is shown in the graph. (**D**) The mean value ± SD of the absolute number of $CD19^+$ $CD5^+$ cells gated on $CD19^+$ in PE, (**E**) in SP, (**F**) in the BM and (**G**) LN of mice described in (A) and (B) is shown in graphs. (**H**) The mean value ± SD of the absolute number of $CD11b^+$ $CSF1R^+$ cells gated on $CD45^+$ in BM of mice described in (A) is shown in graph. (**I**) The mean value

± SD of the absolute number of $CD11b^+$ $PDL1^+$ cells to the whole monocyte pool ($CD11b^+$ $CSF1R^+$) gated on $CD45^+$ in BM of mice described in (A) is shown in graph. (**J**) The mean value ± SD of the absolute number of $CD11b^+$ $Ly6C^{low}$ monocyte subset gated on $CD45^+$ in the BM of mice described in (A) is shown in graph. (**K**) The mean value ± SD of the relative contribution of the $CD11b^+$ $Ly6C^{low}$ monocyte subset gated on $CD45^+$ in the PB of mice described in (A) is shown in graph. (**L**) The mean value ± SD of the absolute number of $CD11b^+$ $CSF1R^+$ cells gated on $CD45^+$ in BM and (**M**) PE of mice described in (B) is shown in graphs. (**N**) The mean value ± SD of the absolute number of $CD11b^+$ PD-$L1^+$ cells to the whole monocyte pool ($CD11b^+$ $CSF1R^+$) gated on $CD45^+$ in BM and (**O**) PE of mice described in (B) is shown in graphs. (**P**) The mean value ± SD of the absolute number of the $CD11b^+$ $Ly6C^{low}$ monocyte subset gated on $CD45^+$ in the BM and (**Q**) PE of mice described in (B) is shown in graphs. *$p < 0.05$, **$p < 0.01$, ***$p < 0.001$, Student *t* test.

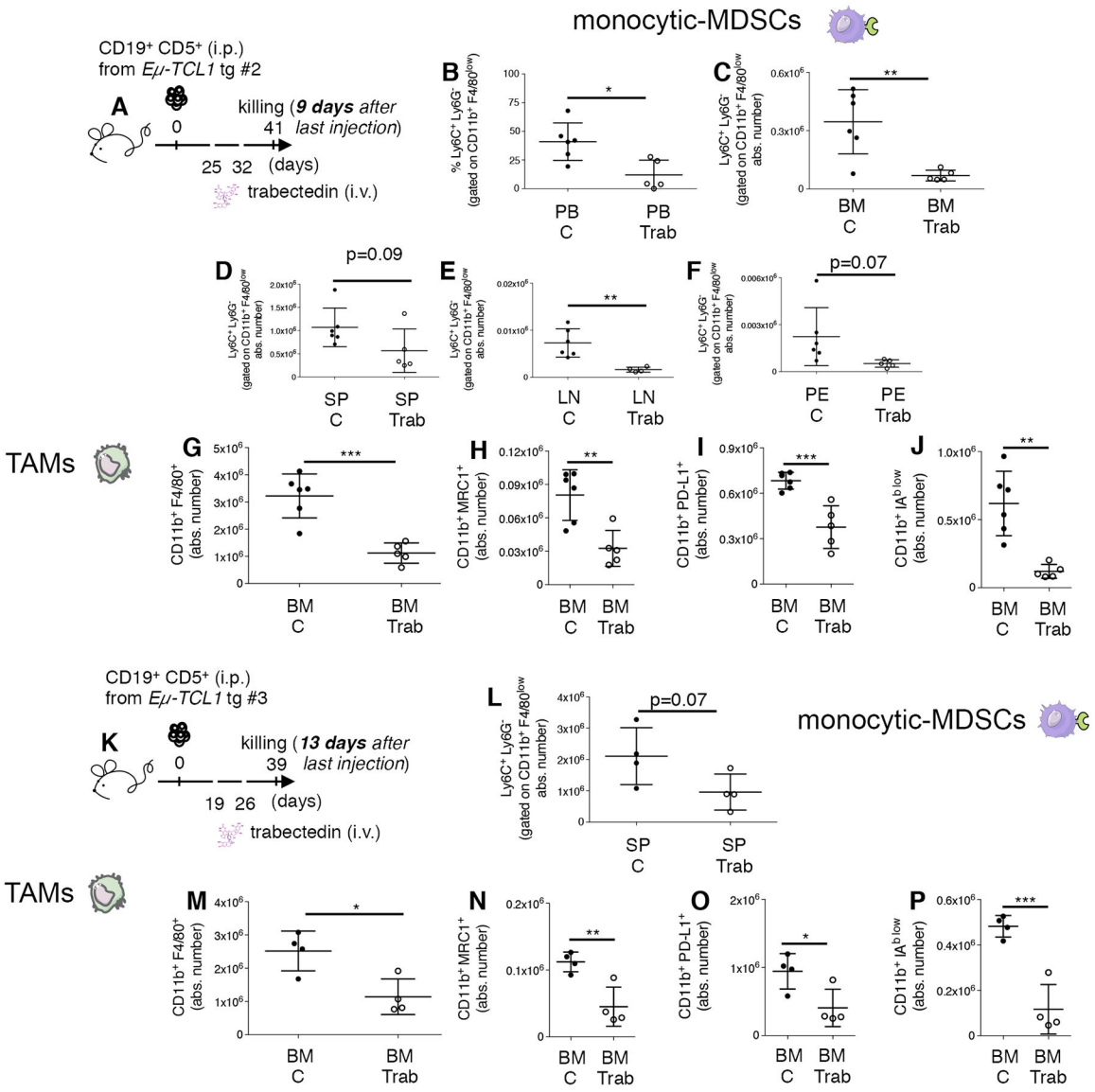

Figure 6. Long-term impact of trabectedin on leukemic cells, M-MDSCs, and TAMs in the TCL1 tg transplantation system

(**A**) C57BL/6 mice i.p. transplanted with leukemic B cells from *Eμ-TCL1* transgenic mouse donor #2, left untreated (n=6, black circles) or i.v. injected (day +25, +32) with 0.15mg/kg of trabectedin (n=5, white circles) were killed on day 41 (9 days after the last trabectedin injection) and analyzed by flow cytometry. (**B**) The mean value ± SD of the relative contribution of monocytic Ly6C$^+$ Ly6G$^-$ gated on CD11b$^+$ F4/80^{low} cells in the PB and of (**C**) the absolute number ± SD of monocytic Ly6C$^+$ Ly6G$^-$ gated on CD11b$^+$ F4/80^{low} cells in BM, (**D**) in SP, (**E**) in LN and (**F**) PE of mice described in (A) is shown in graphs. (**G**) The mean value ± SD of the absolute number of CD11b$^+$ F4/80$^+$ cells gated on CD45$^+$ in BM is shown in graph. (**H**) The mean value ± SD of the absolute number of CD11b$^+$ MRC1$^+$ cells and (**I**) of CD11b$^+$ PD-L1$^+$ cells and (**J**) of CD11b$^+$ IA$^{b\ low}$ cells to the whole macrophage pool (CD11b$^+$ F4/80$^+$) gated on CD45$^+$ in BM of mice described in (A) is shown in graphs. (**K**) C57BL/6 mice i.p. transplanted with leukemic B cells from *Eμ-TCL1*

transgenic mouse donor #3, left untreated (n=4, black circles) or i.v. injected (day +19, +26) with 0.15mg/kg of trabectedin (n=4, white circles) were killed on day 39 (13 days after the last trabectedin injection) and analyzed by flow cytometry. (**L**) The mean value ± SD of the absolute number of monocytic $Ly6C^{+}$ $Ly6G^{-}$ gated on $CD11b^{+}$ $F4/80^{low}$ cells in in SP of mice described in (**K**) is shown in graph. (**M**) The mean value ± SD of the absolute number of $CD11b^{+}$ $F4/80^{+}$ cells gated on $CD45^{+}$ in BM is shown in graph. (**N**) The mean value ± SD of the absolute number of $CD11b^{+}$ $MRC1^{+}$ cells and (**O**) of $CD11b^{+}$ $PD\text{-}L1^{+}$ cells and (**P**) of $CD11b^{+}$ $IA^{b\ low}$ cells to the whole macrophage pool ($CD11b^{+}$ $F4/80^{+}$) gated on $CD45^{+}$ in BM of mice described in (K) is shown in graphs.*$p < 0.05$, **$p < 0.01$, ***$p < 0.001$, Student's t test.

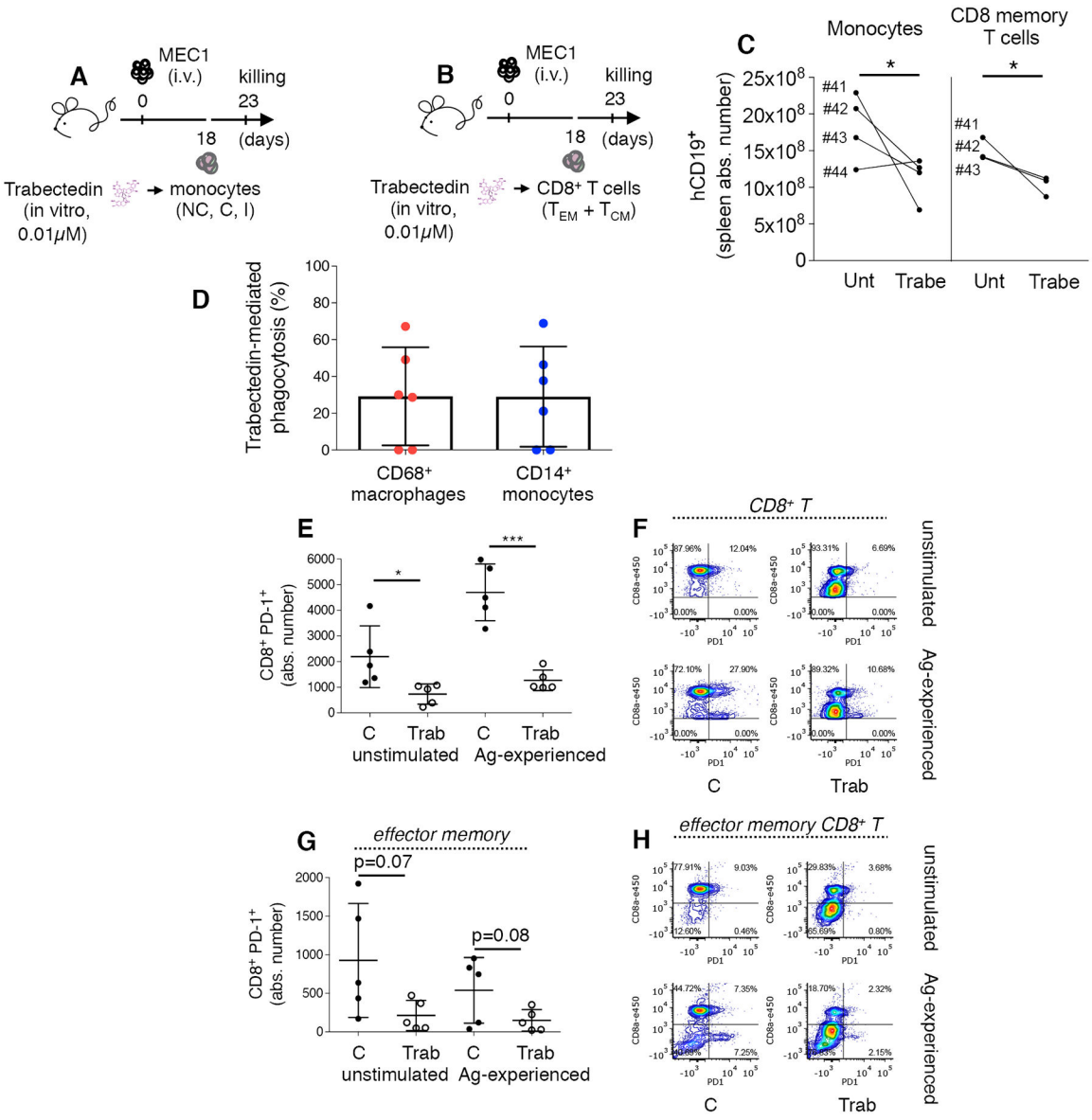

Figure 7. In vivo and in vitro antitumor activity of patient-derived T cells and monocytes/ macrophages

(**A-B**) Rag2$^{-/-}\gamma c^{-/-}$ mice i.v. injected with MEC1 cells (day 0) were adoptively transferred on day 18 with monocytes (i.v.: 35.000–156.000 cells depending on the patient, including NC, C and I subsets) or CD8$^+$ memory cells (i.v.: 36.000–226.000 cells depending on the patient, including T_{EM} and T_{CM} cells) separated from the PBMCs of patients 41–44 (Supplementary Table S2) and in vitro pre-treated with 0.01μM trabectedin for 15h. Mice injected with the same patient sample cells (either treated or untreated, n=4) received the same number of cells and were killed at day 23. (**C**) The mean value ± SD of the absolute number of hCD19$^+$ in the SP from mice transplanted with monocytes (left panel) and T-cells (right panel) is shown in graph. *p < 0.05, Student's t test. (**D**) Monocytes (including NC, C and I) from patient 43 and 45–49 (n=6) were separated by cell-sorting and co-incubated with VPD - labeled MEC1 cells at effector target ratio 1:1 in the presence or absence of 0.01 μM

trabectedin for 16h. The percentage of viable MEC1 target cells was measured by flow cytometry to determine absolute numbers of surviving MEC1 cells. The percentage of trabectedin-mediated phagocytosis by $CD68^+$ macrophages and $CD14^+$ monocytes was calculated as described in the Methods. (**E-H**) $CD8^+$ T lymphocytes (including T_{EM} and T_{CM}) from PBMCs of patients 45–49 (n=5) were separated by cell-sorting, co-incubated in vitro with heated-MEC1 cells (at effector target ratio 2:1) to induce tumor-antigen specific T cell response (Ag-experienced) in absence (C) or presence (Trab) of 0.01μM trabectedin for 15h. (**E**) The mean value ± SD of the absolute number of PD-1^+ T cells to the whole $CD8^+$ T cell pool gated on live cells is shown in graph. *$p < 0.05$, ***$p < 0.001$, Student's t test. (**F**) Flow cytometry detection of PD-1 by $CD8^+$ T cells from representative patient 46. The percentage of PD-1 expressing cells is indicated. (**G**) The mean value ± SD of the absolute number of PD-1^+ cells to the T_{EM} cell pool gated on $CD8^+$ T cells is shown in graph. (**H**) Flow cytometry detection of PD-1 on $CD8^+$ T_{EM} cells from representative patient 46. The percentage of PD-1 expressing cells is indicated.